

# Shape Functions, Derivatives, and Integration

## 6.1 Introduction

In the previous chapter we found that the quasi-harmonic equation created a weak form that contained derivatives of the dependent variable up to first order. Indeed we will find that there is a large class of problems which have equations which have no more than second derivatives of the dependent variables and thus their weak form will contain no more than first derivatives of the dependent variable and arbitrary function. All such forms will require the use of  $C_0$  shape functions for the approximate solution by a finite element method. Thus, in this chapter we present the development of shape functions for some general families of  $C_0$  interpolations. Both two- and three-dimensional forms are considered. With the general families available we are then able to consider their use to solve problems in elasticity, plates, and shells. To this end, we note that these functions must satisfy the following conditions:

1. Be such that continuity is achieved at each point on the interface between adjacent elements.
2. Include complete linear polynomials such that constant derivatives may be obtained in each element.

These two conditions are quite easy to achieve for two-dimensional elements that have triangular or quadrilateral shape and for elements with three-dimensional tetrahedral, wedge, or hexahedral forms.

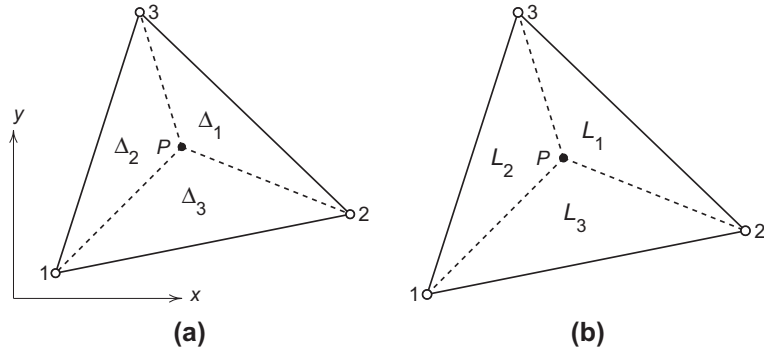
The shape functions presented below are described by local nodes with each local node associated to a specific global node during the assembly process as described in previous chapters.

## 6.2 Two-dimensional shape functions

### 6.2.1 Shape functions for triangles

#### 6.2.1.1 *Triangle with three nodes*

As an example let us consider again the two-dimensional plane problem for which a simple set of  $C_0$  functions for a parameter  $\phi$  may be constructed from linear polynomials over three-node triangles as shown in Fig. 6.1a. The three shape functions for

**FIGURE 6.1**

Triangular element with area and baricentric parent coordinates: (a) subareas of triangle and (b) parent coordinates.

the triangle with nodal coordinates  $x_a, y_a$ , developed in Section 5.1.2, are given by

$$N_a(x, y) = \frac{1}{2\Delta} (a_a + b_a x + c_a y), \quad a = 1, 2, 3$$

where

$$\begin{aligned} a_1 &= x_2 y_3 - x_3 y_2, & b_1 &= y_2 - y_3, & c_1 &= x_3 - x_2 \\ a_2 &= x_3 y_1 - x_1 y_3, & b_2 &= y_3 - y_1, & c_2 &= x_1 - x_3 \\ a_3 &= x_1 y_2 - x_2 y_1, & b_3 &= y_1 - y_2, & c_3 &= x_2 - x_1 \end{aligned}$$

and  $\Delta = (x_1 b_1 + x_2 b_2 + x_3 b_3)/2$  is the area of the triangle.

Geometrically, the numerator of the shape function is twice the area for the triangle composed of point  $(x, y)$  and two of the nodal coordinates  $x_a, y_a$ . Thus, as shown in Fig. 6.1a, we can define

$$2 \Delta_a(x, y) = a_a + b_a x + c_a y \quad (6.1)$$

and the shape functions become

$$N_a = \frac{\Delta_a(x, y)}{\Delta} \quad (6.2)$$

This ratio also defines a convenient parent coordinate system (Fig. 6.1b) for triangles which is known as *baricentric* or *area* coordinates and was first introduced by the German mathematician August Möbius in 1827 [1]. We shall denote these as

$$L_a = \frac{\Delta_a}{\Delta}, \quad a = 1, 2, 3 \quad (6.3)$$

Since there are three parent coordinates it is necessary to always note that they are constrained by the total area such that

$$L_1 + L_2 + L_3 = 1 \quad (6.4)$$

Using area coordinates the shape functions for the three-node triangle are given by

$$N_a = L_a, \quad a = 1, 2, 3 \quad (6.5)$$

### 6.2.1.2 Higher order triangular elements

The process originally used for the three-node triangle may be performed for triangular elements with more than three nodes. The first three members of the triangular element family are shown in Fig. 6.2. It is useful to note that a complete set of polynomials in two dimensions may be represented on a Pascal triangle as shown in Fig. 6.3. Using a Pascal triangle we note that each complete order of the polynomials exactly matches

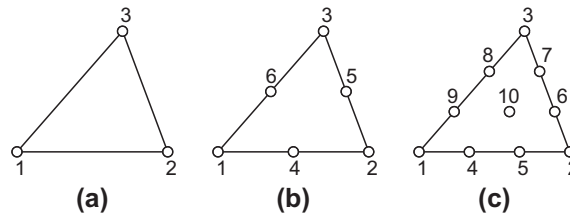


**FIGURE 6.2**

Triangular element family: (a) linear, (b) quadratic, and (c) cubic.

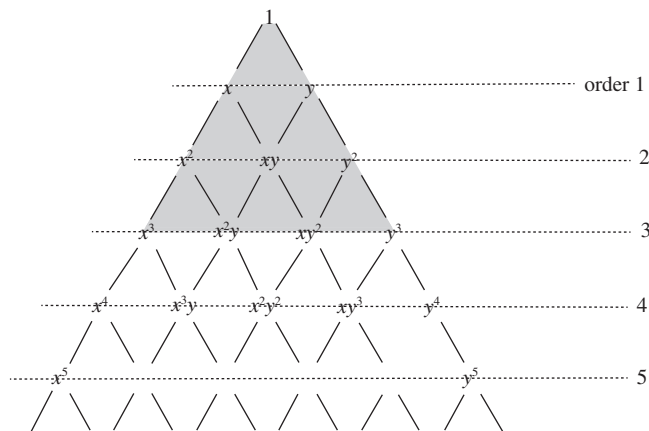


**FIGURE 6.3**

The Pascal triangle (cubic expansion shaded—10 terms).

the number of nodes of the triangle with the same order. Thus, the shape functions for a six-node triangle may be obtained using quadratic order polynomials as

$$\hat{\phi}^e = \alpha_1 + x \alpha_2 + y \alpha_3 + x^2 \alpha_4 + xy \alpha_5 + y^2 \alpha_6 \quad (6.6)$$

Pursuing this approach will require the inverse of a  $6 \times 6$  matrix to obtain the expression for the parameters  $\alpha_a$  in terms of the nodal parameters  $\tilde{\phi}_a^e$ . Furthermore, each triangle so constructed must have straight edges in order to satisfy the continuity condition between elements. Thus, we shall find it useful to develop the shape functions directly using area coordinates and, thus, eliminate the need to invert matrices.

To derive shape functions for higher order elements a simple recurrence relation can be derived [2]. However, it is very simple to write an arbitrary triangle of order  $M$  in a direct manner.

Denoting a typical node  $a$  by three numbers  $I, J$ , and  $K$  corresponding to the position of coordinates  $L_{1a}$ ,  $L_{2a}$ , and  $L_{3a}$ , we can write the shape function in terms of three Lagrangian interpolations as [see Eq. (3.39)]

$$N_a = l_I^I(L_1)l_J^J(L_2)l_K^K(L_3) \quad \text{with } I + J + K = M \quad (6.7)$$

In the above  $l_I^I, l_J^J, l_K^K$  are given by expression (3.39), with  $L_1, L_2, L_3$  taking the place of  $\xi$ .

It is easy to verify that the above expression gives

$$N_a = 1 \quad \text{at } L_1 = L_{1I}, \quad L_2 = L_{2J}, \quad L_3 = L_{3K}$$

and zero at all other nodes. The highest term occurring in the expansion is  $L_1^I L_2^J L_3^K$  and as  $I + J + K \equiv M$  for all points the polynomial is also of order  $M$ .

Expression (6.7) is valid for quite arbitrary distributions of nodes of the pattern given in Fig. 6.4 and simplifies if the spacing of the nodal lines is equal (i.e.,  $1/m$ ). The formula was first obtained by Argyris et al. [3] and formalized in a different manner by others [4,5].

The reader can verify the shape functions for the second- and third-order elements as given below and indeed derive ones of any higher order easily.

### 6.2.1.3 Quadratic triangle (Fig. 6.2b)

Corner nodes:

$$N_a = (2L_a - 1)L_a, \quad a = 1, 2, 3$$

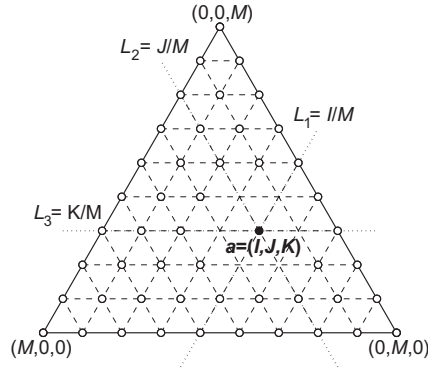
Mid-side nodes:

$$N_4 = 4L_1L_2, \quad N_5 = 4L_2L_3, \quad N_6 = 4L_3L_1$$

### 6.2.1.4 Cubic triangle (Fig. 6.2c)

Corner nodes:

$$N_a = \frac{1}{2}(3L_a - 1)(3L_a - 2)L_a, \quad a = 1, 2, 3$$

**FIGURE 6.4**

A general triangular element.

Mid-side nodes:

$$N_4 = \frac{9}{2}L_1L_2(3L_1 - 1), \quad N_5 = \frac{9}{2}L_1L_2(3L_2 - 1), \quad \text{etc.}$$

The internal node:

$$N_{10} = 27L_1L_2L_3$$

The last shape again is a “bubble” function giving zero contribution along boundaries—this will be found to be useful in other contexts (see the mixed forms in Chapter 10).

The quadratic triangle was first derived by de Veubeke [6] and used later in the context of plane stress analysis by Argyris [7].

## 6.2.2 Shape functions for quadrilaterals

### 6.2.2.1 Quadrilateral with four nodes

In Section 5.1.2 the shape functions for the rectangular element shown in Fig. 6.5a were obtained as

$$\begin{aligned} N_1 &= \frac{1}{4} \left(1 - \frac{x'}{a}\right) \left(1 - \frac{y'}{b}\right), & N_2 &= \frac{1}{4} \left(1 + \frac{x'}{a}\right) \left(1 - \frac{y'}{b}\right) \\ N_3 &= \frac{1}{4} \left(1 + \frac{x'}{a}\right) \left(1 + \frac{y'}{b}\right), & N_4 &= \frac{1}{4} \left(1 - \frac{x'}{a}\right) \left(1 + \frac{y'}{b}\right) \end{aligned}$$

If we let

$$\xi = \frac{x'}{a} \quad \text{and} \quad \eta = \frac{y'}{b}$$

the shape functions on a parent element (viz. Fig. 6.5b) may be written as

$$\begin{aligned} N_1 &= \frac{1}{2}(1 - \xi) \cdot \frac{1}{2}(1 - \eta), & N_2 &= \frac{1}{2}(1 + \xi) \cdot \frac{1}{2}(1 - \eta) \\ N_3 &= \frac{1}{2}(1 + \xi) \cdot \frac{1}{2}(1 + \eta), & N_4 &= \frac{1}{2}(1 - \xi) \cdot \frac{1}{2}(1 + \eta) \end{aligned} \quad (6.8)$$

which we recognize as products of one-dimensional Lagrange interpolations using the parent coordinates  $-1 \leq \xi, \eta \leq 1$ .

### 6.2.2.2 Lagrangian family of quadrilaterals

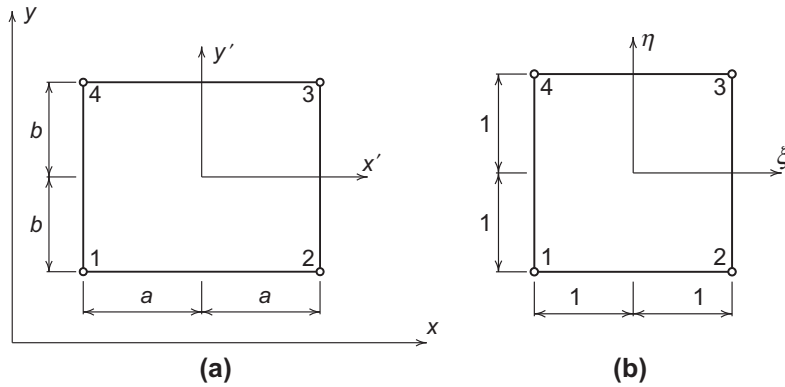
Based on the above a systematic and easy method to generate shape functions for any order of rectangle can be achieved by a simple product of Lagrange polynomials in the two parent coordinates [8–10]. Thus, in two dimensions, if we label the node by its column and row number,  $I, J$ , using the definition of Lagrange polynomials given in (3.39) we have

$$N_a \equiv N_{IJ} = l_I^n(\xi)l_J^m(\eta) \quad (6.9)$$

where  $n$  and  $m$  stand for the number of subdivisions in each direction. Table 6.1 shows how the  $I, J$  values are mapped to the node numbers  $a$  shown in Fig. 6.5. Figure 6.6 shows a few members of this unlimited family where  $m = n$ . For  $m = n = 1$  we obtain the simple result

$$N_a = \frac{1}{4}(1 + \xi_a \xi)(1 + \eta_a \eta)$$

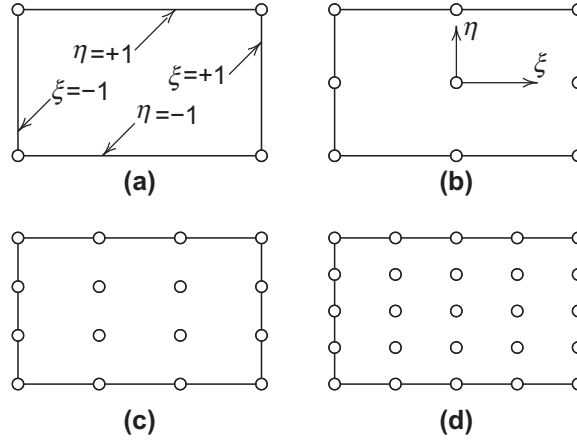
in which  $\xi_a, \eta_a$  are the normalized coordinates at node  $a$ .



**FIGURE 6.5**

Rectangular element geometry and local node numbers: (a) global coordinates and (b) parent coordinates.

Table 6.1 Numbering for Four-Node Rectangle				
Label	Node Numbers			
a	1	2	3	4
I	1	2	2	1
J	1	1	2	2

**FIGURE 6.6**

Four elements of the Lagrangian family: (a) linear, (b) quadratic, (c) cubic, and (d) quartic.

### 6.2.2.3 “Quadratic” element (Fig. 6.6b)

Products of one-dimensional quadratic Lagrange interpolations yield the following:

Corner nodes:

$$N_a = \frac{1}{4} \xi \eta (\xi + \xi_a)(\eta + \eta_a)$$

Mid-side nodes:

$$\xi_a = 0, \quad N_a = \frac{1}{2} \eta (1 - \xi^2)(\eta + \eta_a)$$

$$\eta_a = 0, \quad N_a = \frac{1}{2} \xi (\xi + \xi_a)(1 - \eta^2)$$

Center node:

$$N_a = (1 - \xi^2)(1 - \eta^2)$$

Indeed, if we examine the polynomial terms present in a situation where  $n = m$  we observe in Fig. 6.7, based on the Pascal triangle, that a large number of polynomial

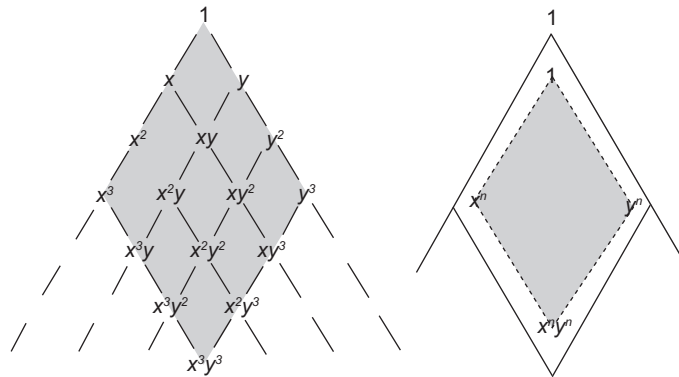


**FIGURE 6.7**

Terms generated by a Lagrangian expansion of order  $3 \times 3$  [or  $m \times n$  using Eq. (6.9)]. The shaded region shows complete polynomials of order 3 and  $n$ .

terms is present above those needed for a complete expansion [4]. However, when mapping of shape functions to more general shapes is considered (viz. Section 6.5) some advantages occur for this family.

#### 6.2.2.4 Serendipity family of quadrilaterals

For some classes of problems it is more efficient to make the functions dependent on nodal values placed mostly on the element boundary. Consider, for instance, the first four elements of Fig. 6.8. In each a progressively increasing and equal number of

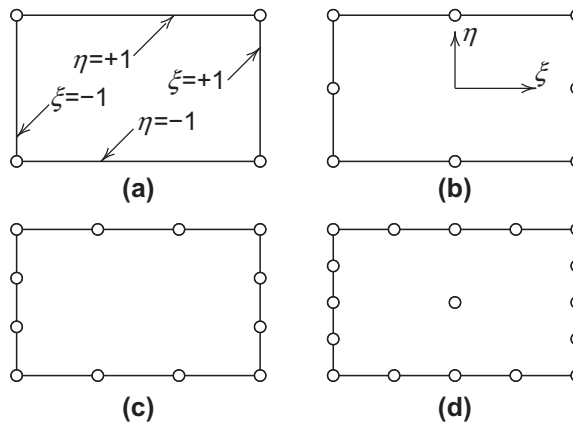


**FIGURE 6.8**

Four elements of the serendipity family: (a) linear, (b) quadratic, (c) cubic, and (d) quartic.



nodes is placed on the element boundary. The variation of the function on the edges to ensure continuity is linear, parabolic, and cubic in increasing element order.

To achieve the shape function for the first element it is obvious that a product of linear Lagrangian polynomials may again be used. Indeed this element is identical to the Lagrangian one with  $n = 1$  and again all the shape functions may be written as one expression:

$$N_a = \frac{1}{4}(1 + \xi_a \xi)(1 + \eta_a \eta)$$

The reader can verify that the following functions satisfy all the necessary criteria for quadratic and cubic members of the family.

#### 6.2.2.5 “Quadratic” element (Fig. 6.8b)

Corner nodes:

$$N_a = \frac{1}{4}(1 + \xi_a \xi)(1 + \eta_a \eta)(\xi_a \xi + \eta_a \eta - 1) \quad (6.10a)$$

Mid-side nodes:

$$\begin{aligned} \xi_a = 0, \quad N_a &= \frac{1}{2}(1 - \xi^2)(1 + \eta_a \eta) \\ \eta_a = 0, \quad N_a &= \frac{1}{2}(1 + \xi_a \xi)(1 - \eta^2) \end{aligned} \quad (6.10b)$$

#### 6.2.2.6 “Cubic” element (Fig. 6.8c)

Corner nodes:

$$N_a = \frac{1}{32}(1 + \xi_a \xi)(1 + \eta_a \eta)[9(\xi^2 + \eta^2) - 10] \quad (6.11a)$$

Mid-side nodes:

$$\begin{aligned} \xi_a = \pm 1 \quad \text{and} \quad \eta_a = \pm \frac{1}{3} \\ N_a = \frac{9}{32}(1 + \xi_a \xi)(1 - \eta^2)(1 + 9\eta_a \eta) \end{aligned} \quad (6.11b)$$

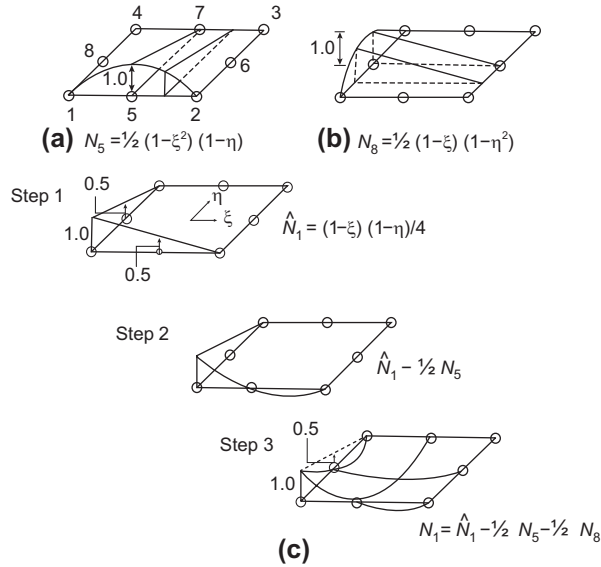
and

$$\begin{aligned} \xi_a = \pm \frac{1}{3} \quad \text{and} \quad \eta_a = \pm 1 \\ N_a = \frac{9}{32}(1 - \xi^2)(1 + 9\xi_a \xi)(1 + \eta_a \eta) \end{aligned} \quad (6.11c)$$

which all satisfy the requirement

$$N_a(\xi_b, \eta_b) = \delta_{ab} = \begin{cases} 1, & a = b \\ 0, & a \neq b \end{cases} \quad (6.11d)$$

The above functions were originally derived by inspection, and progression to yet higher members is difficult and requires some ingenuity [8,9]. It was therefore appropriate to name this family “serendipity” after the famous princes of Serendip noted for their chance discoveries (Horace Walpole, 1754).

**FIGURE 6.9**

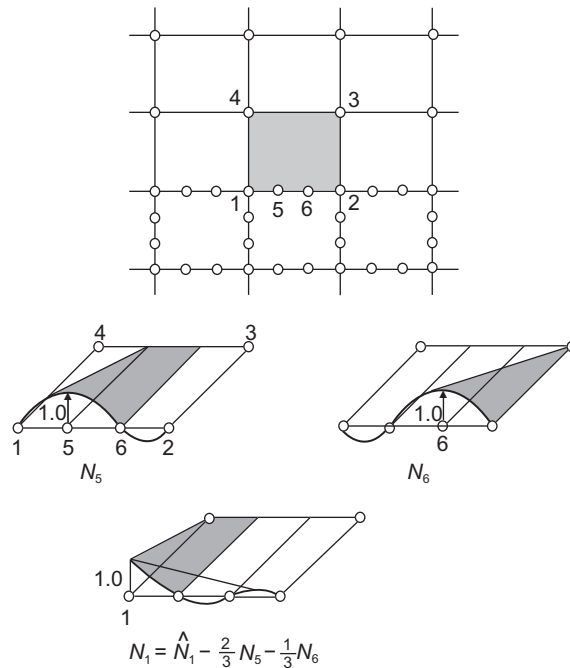
Systematic generation of “serendipity” shape functions.

However, a quite systematic way of generating the “serendipity” shape functions can be devised, which becomes apparent from Fig. 6.9 where the generation of a quadratic  $\times$  linear type suffices to determine  $N_a$  at nodes 5 to 8.  $N_5$  to  $N_8$  are shown in Fig. 6.9a and b. For a *corner* node, such as Fig. 6.9c, we start with a bilinear Lagrangian family  $\hat{N}_1$  and note immediately that while  $\hat{N}_1 = 1$  at node 1, it is not zero at nodes 5 or 8 (step 1). Successive subtraction of  $1/2 N_5$  (step 2) and  $1/2 N_8$  (step 3) ensures that a zero value is obtained at these nodes. The reader can verify that the final expressions obtained coincide with those of Eqs. (6.10a) and (6.10b).

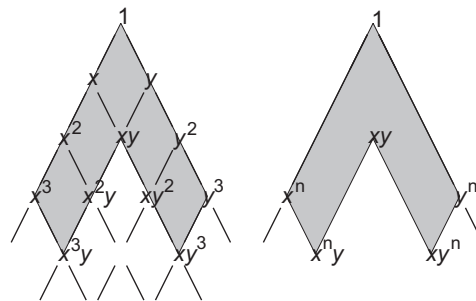
As a starting point we observe that for *mid-side* nodes a Lagrangian interpolation of a quadratic  $\times$  linear type suffices to determine  $N_a$  at nodes 5 to 8.  $N_5$  to  $N_8$  are shown in Fig. 6.9a and b. For a *corner* node, such as Fig. 6.9c, we start with a bilinear Lagrangian family  $\hat{N}_1$  and note immediately that while  $\hat{N}_1 = 1$  at node 1, it is not zero at nodes 5 or 8 (step 1). Successive subtraction of  $1/2 N_5$  (step 2) and  $1/2 N_8$  (step 3) ensures that a zero value is obtained at these nodes. The reader can verify that the final expressions obtained coincide with those of Eqs. (6.10a) and (6.10b).

Indeed, it should now be obvious that for all higher order elements the *mid-side* and *corner* shape functions can be generated by an identical process. For the former a simple multiplication of  $m$ th order and first-order Lagrangian interpolations suffices. For the latter a combination of bilinear corner functions, together with appropriate fractions of mid-side shape functions to ensure zero at appropriate nodes, is necessary.

It is also quite easy to generate shape functions for elements with different numbers of nodes along each side by a similar systematic algorithm. This may be very desirable if a transition between elements of different order is to be achieved, enabling a different order of accuracy in separate sections of a large problem to be studied. Figure 6.10 illustrates the necessary shape functions for a cubic/linear transition. Use of such special elements was first introduced in Ref. [11], but the simpler formulation used here is that of Ref. [4].


**FIGURE 6.10**

Shape functions for a transition “serendipity” element, cubic/linear.


**FIGURE 6.11**

Terms generated by edge-shaped functions in serendipity-type elements ( $3 \times 3$  and  $n \times n$ ).

With the mode of generating shape functions for this class of elements available it is immediately obvious that fewer degrees of freedom are now necessary for a given complete polynomial expansion. Figure 6.11 shows this for a cubic element where only two surplus terms arise (as compared with six surplus terms in a Lagrangian of the same degree). However, when mapping to general quadrilateral shape is introduced in Section 6.5 some of these advantages are lost, rendering the Lagrangian form of interpolation more advantageous.

It is immediately evident, however, that the functions generated by nodes placed only along the edges will not generate complete polynomials beyond cubic order. For higher order ones it is necessary to supplement the expansion by internal nodes or by the use of “node-less” variables which contain appropriate polynomial terms. For example in the next quartic member [12] of this family a central node is added [viz. Fig. 6.8d] so that all terms of a complete fourth-order expansion will be available. This central node adds a shape function  $(1 - \xi^2)(1 - \eta^2)$  which is zero on all outer boundaries and coincides with the internal function used in the quadratic Lagrangian element. Once interior nodes are added it is necessary to modify the corner and mid-side shape functions to preserve the Kronecker delta property (6.11d). However, one may also consider the interior nodes to be hierarchical (viz. Section 3.6).

The reader can verify that at element edges all the above two-dimensional shape functions are expressed entirely by nodal parameters on the edge. Thus, matching values at nodes of contiguous edges ensures the required  $C_0$  continuity.

### 6.3 Three-dimensional shape functions

For interelement continuity the simple rules given previously for edges have to be modified. What is necessary to achieve such continuity is that *along a whole face of an element the nodal values define a unique variation of the unknown function*. In all the elements described below each face will be a two-dimensional interpolation of triangular or quadrilateral shape. Moreover, the face will be described by nodal parameters on the face. Thus, if the nodes on faces of contiguous elements match we are assured that  $C_0$  compatibility is ensured over the whole face.

#### 6.3.1 Tetrahedral elements

The tetrahedral family shown in Fig. 6.12 not surprisingly exhibits properties similar to those of the triangle family as deduced in the previous chapter. Firstly, once again complete polynomials in three coordinates are achieved at each stage. Secondly, as faces are divided in a manner identical with that of the previous triangles, the same order of polynomial in two coordinates in the plane of the face is achieved and element compatibility ensured. Finally, no surplus terms in the polynomial occur.

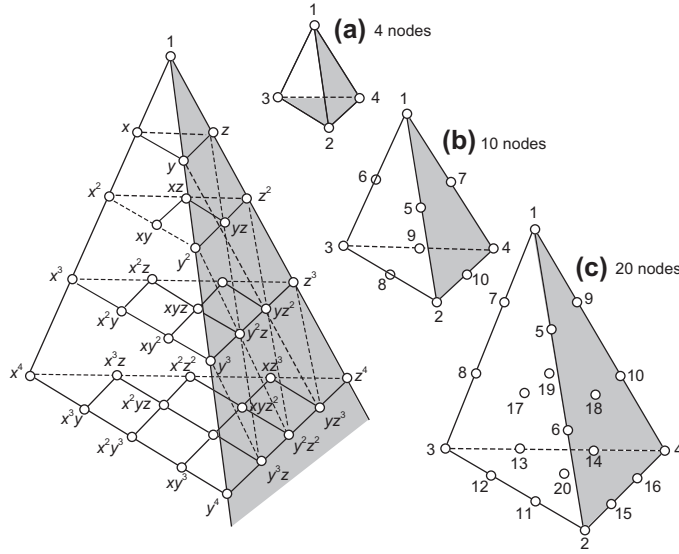
##### 6.3.1.1 Tetrahedron with four nodes

For three-dimensional problems a simple tetrahedron-shaped element was developed in Section 5.1.3 with shape functions given in (5.25) by

$$N_a(x, y, z) = \frac{1}{6V} (a_a + b_a x + c_a y + d_a z), \quad a = 1, 2, 3, 4$$

The above form permits the generalization of area coordinates to *volume coordinates* expressed by  $L_1, L_2, L_3, L_4$ , where

$$L_a = \frac{V_a}{V}, \quad a = 1, 2, 3, 4$$

**FIGURE 6.12**

The tetrahedral family: (a) linear, (b) quadratic, and (c) cubic.

In the above  $V$  is the volume of the tetrahedron with vertices 1234 and  $V_1, V_2, V_3, V_4$  are volumes of the tetrahedron 432P, 413P, 421P, 123P, respectively, that are expressed by

$$6V_a = a_a + b_a x + c_a y + d_a z$$

The subvolume  $V_1$  is shown shaded in Fig. 6.13b. The volume coordinates must satisfy the constraint

$$\sum_{i=1}^4 L_i = L_1 + L_2 + L_3 + L_4 = 1 \quad (6.12)$$

The shape functions for a four-node tetrahedron in terms of volume coordinates are given by

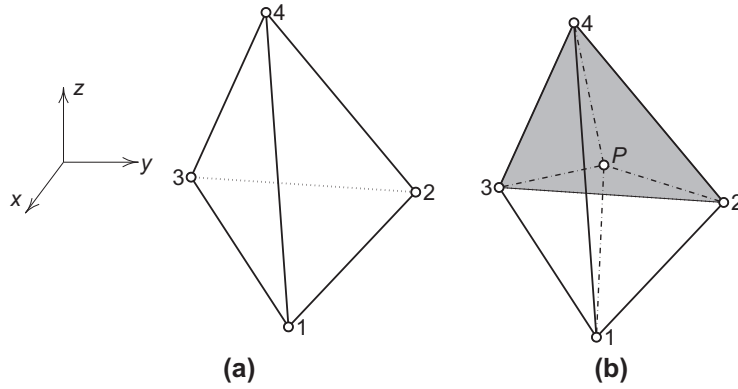
$$N_a = L_a, \quad a = 1, 2, 3, 4 \quad (6.13)$$

This form will be used later in a parametric mapping approach as introduced for the one-dimensional problem in Section 3.5.

To show  $C_0$  continuity between contiguous tetrahedra each face must be described in terms its degrees of freedom. This is trivial to show for the four-node tetrahedron since on each face one of the volume coordinates is zero. For example on the face 123 in Fig. 6.13a the value of  $L_4$  is zero and an interpolation is given by

$$\hat{\phi}^e = N_1(L_1) \tilde{\phi}_1^e + N_2(L_1) \tilde{\phi}_2^e + N_3(L_1) \tilde{\phi}_3^e$$

which is the interpolation in area coordinates for the face. Since this is a linear function it is obvious that continuity is preserved with any adjacent element.

**FIGURE 6.13**

Tetrahedron element. Volume and baricentric coordinates: (a) four-node tetrahedron and (b)  $V_1$  for 432P.

### 6.3.1.2 Higher order tetrahedrons

Formulae for shape functions of higher order tetrahedra are derived in precisely the same manner as for the triangles by establishing appropriate Lagrange-type formulae similar to Eq. (6.7). The result is

$$N_a = l_I^I(L_1)l_J^J(L_2)l_K^K(L_3)l_L^L(L_4) \quad \text{with } I + J + K + L = M \quad (6.14)$$

where  $M$  is the order of the tetrahedron.

The reader may verify the following shape functions for the quadratic and cubic order cases.

### 6.3.1.3 “Quadratic” tetrahedron (Fig. 6.12b)

Corner nodes:

$$N_a = L_a(2L_a - 1), \quad a = 1, 2, 3, 4$$

Mid-edge nodes:

$$\begin{aligned} N_5 &= 4L_2L_1, & N_6 &= 4L_3L_1, & N_7 &= 4L_4L_1 \\ N_8 &= 4L_2L_3, & N_9 &= 4L_3L_4, & N_{10} &= 4L_4L_2 \end{aligned}$$

### 6.3.1.4 “Cubic” tetrahedron (Fig. 6.12c)

Corner nodes:

$$N_a = \frac{1}{2}L_a(3L_a - 1)(3L_a - 2), \quad a = 1, 2, 3, 4$$

Mid-edge nodes:

$$N_5 = \frac{9}{2}L_1L_2(3L_1 - 1), \quad N_6 = \frac{9}{2}L_1L_2(3L_2 - 1), \quad \text{etc.}$$

Mid-face nodes:

$$N_{17} = 27L_1L_2L_3, \quad \text{etc.}$$

### 6.3.2 Hexagon elements: Brick family

#### 6.3.2.1 Hexagon with eight nodes

For a three-dimensional problem we consider the rectangular brick shown in Fig. 6.14. The development of shape functions follows the procedure used for the four-node quadrilateral in Section 6.2.2.1. Introducing the coordinates  $x'$ ,  $y'$ ,  $z'$  we may write a polynomial expression for  $\phi$  as

$$\hat{\phi}^e = \begin{bmatrix} 1 & x & y & z & xy & yz & zx & xyz \end{bmatrix} \begin{Bmatrix} \alpha_1 \\ \alpha_2 \\ \alpha_3 \\ \alpha_4 \\ \alpha_5 \\ \alpha_6 \\ \alpha_7 \\ \alpha_8 \end{Bmatrix} \quad (6.15)$$

Introducing the nondimensional (parent coordinates)

$$\xi = \frac{x'}{a}, \quad \eta = \frac{y'}{b}, \quad \text{and} \quad \zeta = \frac{z'}{c} \quad (6.16)$$

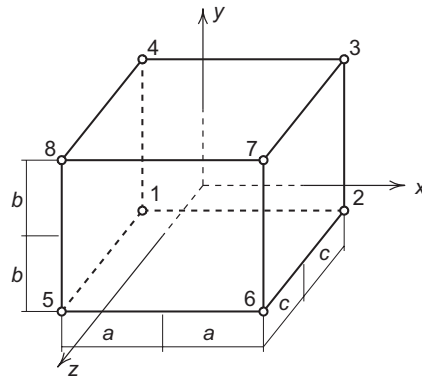


**FIGURE 6.14**

Brick element geometry and local node numbers.

the coefficients  $\alpha_a$  may be obtained in the identical manner used above for the two-dimensional rectangle. The reader can verify that the result is

$$\begin{aligned} N_1 &= \frac{1}{8}(1-\xi)(1-\eta)(1-\zeta), & N_5 &= \frac{1}{8}(1-\xi)(1-\eta)(1+\zeta) \\ N_2 &= \frac{1}{8}(1+\xi)(1-\eta)(1-\zeta), & N_6 &= \frac{1}{8}(1+\xi)(1-\eta)(1+\zeta) \\ N_3 &= \frac{1}{8}(1+\xi)(1+\eta)(1-\zeta), & N_7 &= \frac{1}{8}(1+\xi)(1+\eta)(1+\zeta) \\ N_4 &= \frac{1}{8}(1-\xi)(1+\eta)(1-\zeta), & N_8 &= \frac{1}{8}(1-\xi)(1+\eta)(1+\zeta) \end{aligned} \quad (6.17)$$

which we may recognize again as products of linear Lagrange interpolations in the parent coordinates  $\xi, \eta, \zeta$ .

### 6.3.2.2 Brick elements: Lagrangian family

In a precisely analogous way to that given in Section 6.2.2.2 equivalent Lagrangian family elements of the three-dimensional brick type can be described. Shape functions for such elements will be generated by a direct product of three Lagrange polynomials. Extending the notation of Eq. (6.9) we now have the interpolations in the parent element given by

$$N_a \equiv N_{IJK} = l_I^n(\xi)l_J^m(\eta)l_K^p(\zeta) \quad (6.18)$$

for  $n, m$ , and  $p$  subdivisions along each side and with

$$-1 \leq \xi, \eta, \zeta \leq 1$$

This element again is suggested by Zienkiewicz et al. [9] and elaborated upon by Argyris et al. [10]. All the remarks about internal nodes are applicable here. The first three of the three-dimensional Lagrangian family are shown in Fig. 6.15a.

### 6.3.2.3 “Linear” element (eight nodes) (Fig. 6.15a)

The linear element has shape functions defined by the product of linear Lagrangian interpolations and is given by

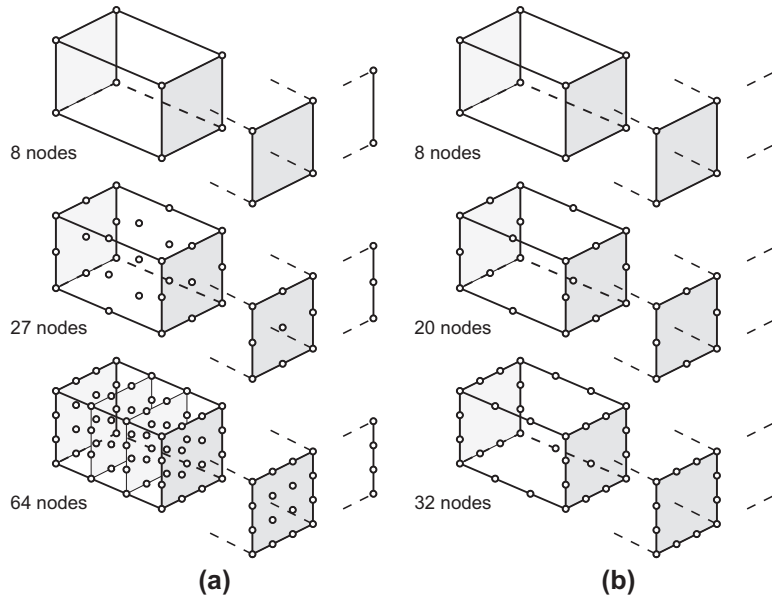
$$N_a(\xi, \eta, \zeta) = \frac{1}{8}(1 + \xi_a \xi)(1 + \eta_a \eta)(1 + \zeta_a \zeta)$$

If we order the nodal numbers with the  $\xi_a, \eta_a, \zeta_a$  as defined in Table 6.2, on face  $\zeta = 1$  the shape functions for nodes 1 to 4 are zero and, thus, the interpolation on the face is given by

$$\hat{\phi}^e = \sum_{a=5}^8 N_a(\xi, \eta, 1) \tilde{\phi}_a^e \equiv \sum_{a=5}^8 N_a(\xi, \eta) \tilde{\phi}_a^e$$

The three-dimensional shape functions  $N(\xi, \eta, 1)$  are precisely the two-dimensional shape functions  $N_a(\xi, \eta)$ . Thus, we are assured that matching the face with a face of the same shape and global node numbers on an adjacent element will assure  $C_0$  continuity.



**FIGURE 6.15**

Linear, quadratic, and cubic right prisms with corresponding sheet and line elements (extra shading on 64-node element to show node location more clearly): (a) Lagrangian family and (b) serendipity family.

<b>Table 6.2</b> Numbering for Eight-Node Brick								
<b>Label</b>	<b>Node Numbers</b>							
<b>a</b>	<b>1</b>	<b>2</b>	<b>3</b>	<b>4</b>	<b>5</b>	<b>6</b>	<b>7</b>	<b>8</b>
$\xi_a$	1	2	2	1	1	2	2	1
$\eta_a$	1	1	2	2	1	1	2	2
$\zeta_a$	1	1	1	1	2	2	2	2

#### 6.3.2.4 Brick elements: “Serendipity” family

The serendipity family of elements shown in Fig. 6.15b is precisely equivalent to that of Fig. 6.8 for the two-dimensional case [8, 11, 13]. Using now three coordinates and otherwise following the terminology used for quadrilaterals, we have the following shape functions.

#### 6.3.2.5 “Linear” element (eight nodes) (Fig. 6.15b)

$$N_a = \frac{1}{8}(1 + \xi_a \xi)(1 + \eta_a \eta)(1 + \zeta_a \zeta)$$

which is identical with the linear Lagrangian element.

**6.3.2.6 “Quadratic” element (20 nodes) (Fig. 6.15b)**

Corner nodes:

$$N_a = \frac{1}{8}(1 + \xi_a \xi)(1 + \eta_a \eta)(1 + \zeta_a \zeta)(\xi_a \xi + \eta_a \eta + \zeta_a \zeta - 2)$$

Typical mid-side node:

$$\begin{aligned} \xi_a &= 0, \quad \eta_a = \pm 1, \quad \zeta_a = \pm 1 \\ N_a &= \frac{1}{4}(1 - \xi^2)(1 + \eta_a \eta)(1 + \zeta_a \zeta) \end{aligned}$$

**6.3.2.7 “Cubic” elements (32 nodes) (Fig. 6.15b)**

Corner node:

$$N_a = \frac{1}{64}(1 + \xi_a \xi)(1 + \eta_a \eta)(1 + \zeta_a \zeta)[9(\xi^2 + \eta^2 + \zeta^2) - 19]$$

Typical mid-side node:

$$\begin{aligned} \xi_a &= \pm \frac{1}{3}, \quad \eta_a = \pm 1, \quad \zeta_a = \pm 1 \\ N_a &= \frac{9}{64}(1 - \xi^2)(1 + 9\xi_a \xi)(1 + \eta_a \eta)(1 + \zeta_a \zeta) \end{aligned}$$

When  $\zeta_a \zeta = \zeta^2 = 1$  the above expressions reduce to those of Eqs. (6.10a) to (6.11b). Indeed such elements of three-dimensional type can be joined in a compatible manner to two-dimensional sheet or one-dimensional line elements of the appropriate type as shown in Fig. 6.15.

Once again the procedure for generating the shape functions follows that described in Figs. 6.9 and 6.10. Elements with varying degrees of freedom along the edges also can be derived following the same steps.

The equivalent of a Pascal triangle is now a tetrahedron and again we find a small number of surplus degrees of freedom—a situation of even greater magnitude than in two-dimensional analysis.

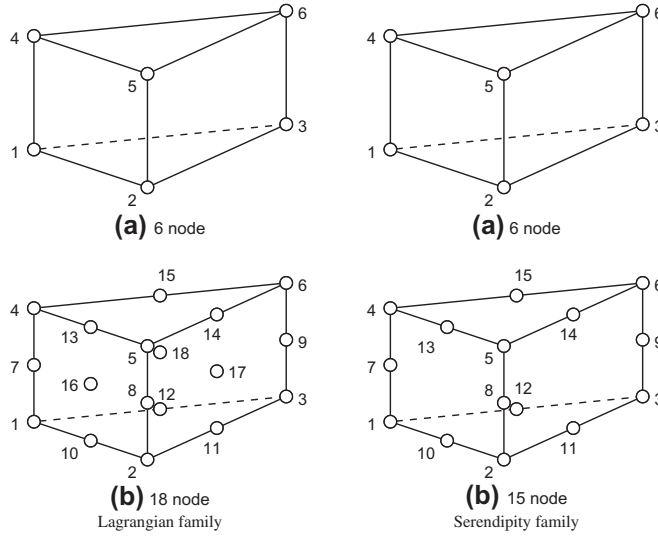
---

**6.4 Other simple three-dimensional elements**

The possibilities of simple shapes in three dimensions are greater, for obvious reasons, than in two dimensions. A quite useful series of elements can, for instance, be based on triangular prisms (wedges) (Fig. 6.16). Here again variants of the product Lagrange approach or of the “serendipity” type can be distinguished. The first element of both families, shown in Fig. 6.16a, is identical and the shape functions are

$$N_a = \frac{1}{2} L_a (1 + \zeta_a \zeta), \quad a = 1, 2, \dots, 6$$

where  $\zeta$  is used as the parent direction perpendicular to triangular faces. For the “quadratic” element illustrated in Fig. 6.16b the shape functions are as follows.

**FIGURE 6.16**

Triangular prism elements for the Lagrangian and serendipity family: (a) linear and (b) quadratic.

### 6.4.1 “Serendipity” quadratic

Corner nodes:

$$N_a = \frac{1}{2}L_a(2L_a - 1)(1 + \zeta_a\zeta) - \frac{1}{2}L_a(1 - \zeta^2), \quad a = 1, 2, \dots, 6$$

Mid-edge of rectangle:

$$N_{a+6} = L_a(1 - \zeta^2), \quad a = 1, 2, 3$$

Mid-edge of triangles:

$$\begin{aligned} N_{10} &= 2L_1L_2(1 - \zeta), & N_{11} &= 2L_2L_3(1 - \zeta), & N_{12} &= 2L_3L_1(1 - \zeta) \\ N_{13} &= 2L_1L_2(1 + \zeta), & N_{14} &= 2L_2L_3(1 + \zeta), & N_{15} &= 2L_3L_1(1 + \zeta) \end{aligned}$$

Similar elements may be developed for higher order elements as well as for the Lagrangian family. Such elements are not purely esoteric but have a practical application as “fillers” in conjunction with 20-node serendipity elements.

A similar wedge combining Lagrangian faces with triangular ones may be developed and used in conjunction with 27-node Lagrangian brick elements.

## 6.5 Mapping: Parametric forms

Once the shape functions are available in terms of parent coordinates we may immediately use the parametric mapping concept introduced in Section 3.5. Indeed, we do not always need to use the same interpolation for coordinates and dependent variables; however an isoparametric mapping is the most convenient since then nodal coordinates and nodal dependent variables are placed at the same physical locations. The use of isoparametric mappings was first used for a four-node quadrilateral element by Taig in 1957 [14]. Figure 6.17a shows the four-node rectangular element in parent coordinates  $\xi, \eta$  and Fig. 6.17b shows the element after a parametric mapping given by

$$\mathbf{x}(\xi, \eta) = \sum_a N'_a(\xi, \eta) \mathbf{x}_a \quad (6.19)$$

where  $N'_a = (1 + \xi_a \xi)(1 + \eta_a \eta)/4$ . The map of the element must be such that all the vertex angles remain less than  $180^\circ$ , otherwise there will be multiple  $\xi, \eta$  that have the same global coordinates  $x, y$  at some points of the element or lie outside the boundary of the quadrilateral. An example of such a mapping is shown for a four-node quadrilateral in Fig. 6.18 where the parts above node 4 are areas with a negative area. Thus, the isoparametric mapping must always be such that single-valued mappings exist. This places restrictions on where the element nodes may be placed. Some curvilinear mappings for solid and surfaces are shown in Fig. 6.19. The use of mapping allows for any general shape to be approximated by the element types described above.

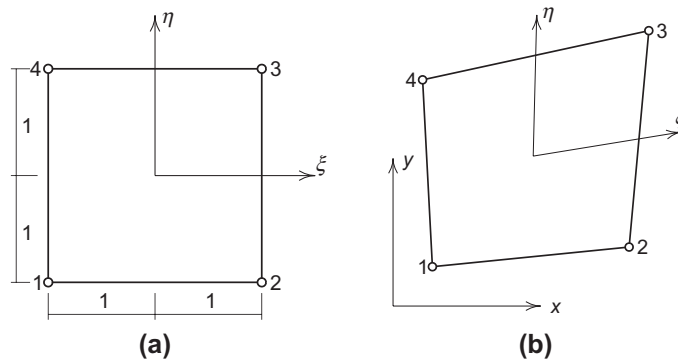


**FIGURE 6.17**

Isoparametric mapping of four-node quadrilateral element: (a) parent coordinates and (b) Global coordinates.

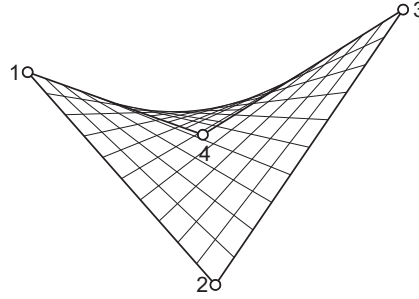


**FIGURE 6.18**  
Inadmissible mapping of four-node quadrilateral element.

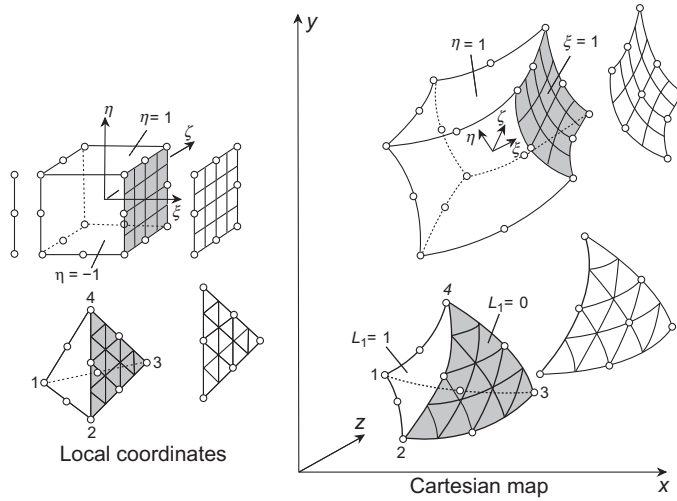


**FIGURE 6.19**  
Isoparametric mapping of solids and surfaces.

The types of parametric mapping that can be considered in an analysis are defined by the relationship between the coordinate interpolation and the dependent variable interpolation. If we denote the mapping by

$$\begin{aligned} \mathbf{x}(\xi_j) &= \sum_a N'_a(\xi_j) \mathbf{x}_a \\ \hat{\phi}(\xi_j) &= \sum_a N_a(\xi_j) \tilde{\phi}_a \end{aligned} \quad (6.20)$$

where  $\xi_j$  are any of the parent coordinates defined above, then we have the following three cases:

- Sub-parametric interpolation:* The order of the interpolation for  $\mathbf{x}$  is lower than that for  $\phi$ .
- Isoparametric interpolation:* The order of the interpolation for  $\mathbf{x}$  is the same as that for  $\phi$ .
- Super-parametric interpolation:* The order of the interpolation for  $\mathbf{x}$  is higher than that for  $\phi$ .

In developing solutions to  $C_0$  problems one may use either “sub-parametric” or “isoparametric” interpolations since either ensures that the polynomials  $1, x, y$  and for three dimensions  $z$  are always available, thus ensuring that constant derivatives can be computed. On the other hand use of “super-parametric” interpolation should generally be avoided.

## 6.6 Order of convergence for mapped elements

If the shape functions are chosen in curvilinear coordinate space so as to observe the usual rules of convergence (continuity and presence of complete first-order polynomials in these coordinates), then convergence will occur. In the case of isoparametric (or sub-parametric) elements a complete linear field is always reproduced (i.e.,  $1, x, y, z$ ) by the curvilinear coordinate expansion, and thus a constant derivative with respect to global coordinates will always exist.

The proof of this is simple. Consider a standard isoparametric expansion

$$\phi = \sum_{a=1}^n N_a \tilde{\phi}_a \equiv \mathbf{N} \tilde{\boldsymbol{\phi}}, \quad \mathbf{N} = \mathbf{N}(\xi, \eta, \zeta) \quad (6.21)$$

with coordinates of nodes defining the transformation as

$$x = \sum N_a x_a, \quad y = \sum N_a y_a, \quad z = \sum N_a z_a \quad (6.22)$$

The question is under what circumstances is it possible for expression (6.21) to define a linear expansion in Cartesian coordinates:

$$\begin{aligned} \phi &= \alpha_1 + \alpha_2 x + \alpha_3 y + \alpha_4 z \\ &\equiv \alpha_1 + \alpha_2 \sum N_a x_a + \alpha_3 \sum N_a y_a + \alpha_4 \sum N_a z_a \end{aligned} \quad (6.23)$$

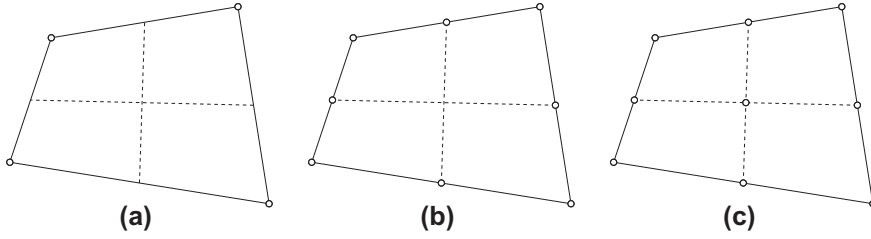
If we take

$$\tilde{\phi}_a = \alpha_1 + \alpha_2 x_a + \alpha_3 y_a + \alpha_4 z_a$$

and compare expression (6.21) with (6.23) we note that identity is obtained between these providing

$$\sum N_a = 1$$

As this is the usual requirement of standard element shape functions [see Eq. (3.51)] we can conclude that *the constant derivative condition will be satisfied for all isoparametric elements.*

**FIGURE 6.20**

Bilinear mapping of sub-parametric quadratic eight- and nine-node elements: (a) four-node mapping, (b) eight-node element, (c) nine-node element.

As sub-parametric elements can always be expressed as specific cases of an isoparametric transformation this result is obviously valid here also.

It is of interest to pursue the argument and to see under what circumstances higher polynomial expansions in Cartesian coordinates can be achieved under various transformations. The simple linear case in which we “guessed” the solution has now to be replaced by considering in detail the polynomial terms occurring in expressions such as (6.21) and (6.23) and establishing conditions for equating appropriate coefficients.

Consider a specific two-dimensional problem: the circumstances under which the bilinear mapped quadrilateral of Fig. 6.20 can fully represent any quadratic Cartesian expansion. We now have

$$x = \sum_{a=1}^4 N'_a x_a, \quad y = \sum_{a=1}^4 N'_a y_a \quad (6.24)$$

and we wish to be able to reproduce

$$\phi = \alpha_1 + \alpha_2 x + \alpha_3 y + \alpha_4 x^2 + \alpha_5 xy + \alpha_6 y^2 \quad (6.25)$$

Noting that the bilinear form of  $N'_a$  contains terms such as 1,  $\xi$ ,  $\eta$ , and  $\xi\eta$ , the above can be written as

$$\phi = \beta_1 + \beta_2 \xi + \beta_3 \eta + \beta_4 \xi^2 + \beta_5 \xi \eta + \beta_6 \eta^2 + \beta_7 \xi \eta^2 + \beta_8 \xi^2 \eta + \beta_9 \xi^2 \eta^2 \quad (6.26)$$

where  $\beta_1$  to  $\beta_9$  depend on the values of  $\alpha_1$  to  $\alpha_6$ .

We shall now try to match the terms arising from the quadratic expansions of the serendipity kind shown in Fig. 6.20b where the interpolation is

$$\phi = \sum_{a=1}^8 N_a \tilde{\phi}_a \quad (6.27)$$

with the appropriate shape functions of the kind defined in Section 6.2.2.4. We can also write (6.27) directly using polynomial coefficients  $b_a$ ,  $a = 1, \dots, 8$ , in place of

the nodal variables  $\tilde{\phi}_a$  (noting the terms occurring in the Pascal triangle) as

$$\phi = b_1 + b_2\xi + b_3\eta + b_4\xi^2 + b_5\xi\eta + b_6\eta^2 + b_7\xi\eta^2 + b_8\xi^2\eta \quad (6.28)$$

It is immediately evident that for arbitrary values of  $\beta_1$  to  $\beta_9$  it is impossible to match the coefficients  $b_1$  to  $b_8$  due to the absence of the term  $\xi^2\eta^2$  in Eq. (6.28). This term is also missing from the cubic serendipity kind, however if higher order quartic expansions were used such matching would evidently be possible and we could conclude that for linearly distorted elements the serendipity family of order 4 or greater will always represent quadratic polynomials in  $x, y$ .

For the nine-node, Lagrangian, (Fig. 6.20c) an expansion similar to (6.27) gives

$$\phi = \sum_{a=1}^9 N_a \tilde{\phi}_a \quad (6.29)$$

which when expressed directly in polynomial coefficients  $b_a, a = 1, \dots, 9$ , yields

$$\phi = b_1 + b_2\xi + b_3\eta + b_4\xi^2 + \dots + b_8\xi^2\eta + b_9\xi^2\eta^2 \quad (6.30)$$

The matching of the coefficients of Eqs. (6.30) and (6.26) can be made directly.

We can conclude therefore that nine-node elements better represent Cartesian polynomials (when distorted linearly) and therefore are generally preferable in modeling smooth solutions. This matter was first presented by Wachspress [15] but the simple proof presented above is due to Crochet [16].

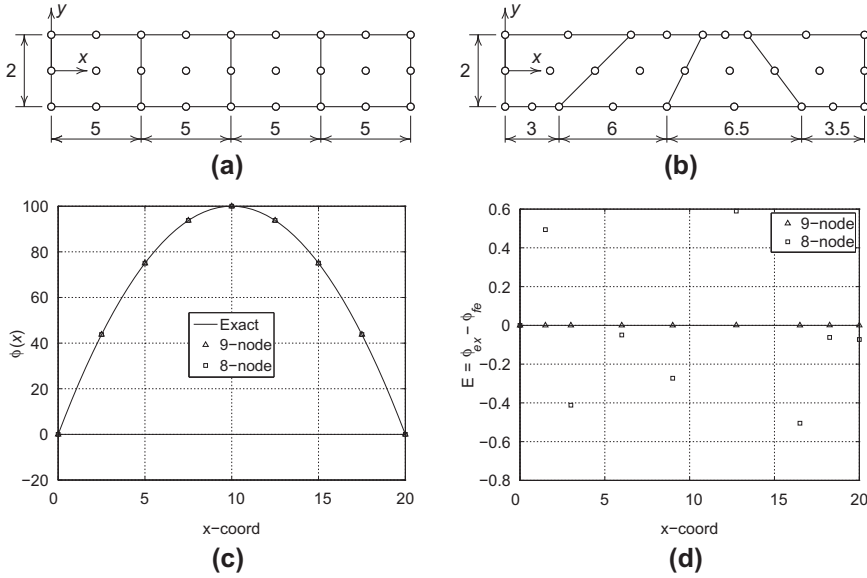
An example of this is given in Fig. 6.21 where we consider the results of a finite element calculation with eight- and nine-node elements, respectively, used to reproduce a simple quasi-harmonic solution in which we know that the exact answers are quadratic. The data for the quasi-harmonic solution is  $k = 10$ ,  $Q = 20$ ,  $\bar{q}_n$  is zero on the top and bottom,  $\bar{q}_n = -200$  on the right boundary, and  $\bar{\phi} = 0$  on the left boundary. The exact solution is given by

$$\phi(x, y) = 20x - x^2$$

With no distortion both elements give exact results but when distorted only the nine-node element does so, with the eight-node element giving errors as shown in Fig. 6.21d. These errors also appear in the computed flux. While the errors are small for this problem, in elasticity applications the errors can be much larger. Similar arguments will lead to the conclusion that in three dimensions again only the Lagrangian 27-node element is capable of reproducing fully a quadratic function in Cartesian coordinates when trilinearly distorted (i.e., using the mapping for  $N'_a$  for the eight-node hexahedron).

Lee and Bathe [17] investigate the problem for cubic and quartic serendipity and Lagrangian quadrilateral elements and show that under bilinear distortions the *full order* cartesian polynomial terms remain in Lagrangian elements but not in serendipity ones. They also consider edge distortion and show that this polynomial order is always lost. Additional discussion of such problems is also given by Wachspress [15].



**FIGURE 6.21**

Quadratic eight-node serendipity and nine-node Lagrangian elements in regular and distorted form. Distribution of  $\phi$  for quasi-harmonic solution with quadratic variation in  $x$ : (a) regular mesh, (b) distorted mesh, (c)  $\phi$  solution, and (d) error  $\phi$ .

## 6.7 Computation of global derivatives

In order to define the gradient matrices appearing in weak forms we need to compute derivatives of the shape functions with respect to the global coordinates  $x$ ,  $y$ ,  $z$  (or for the axisymmetric problem with respect to  $r$ ,  $z$ ). Consider, for instance, a two-dimensional case with the set of local coordinates  $\xi = [\xi, \eta]$  and a corresponding set of global coordinates  $\mathbf{x} = [x, y]$ . By the usual chain rules of partial differentiation we can write the  $x$  and  $y$  derivatives of any function  $f(\xi, \eta)$  as

$$\begin{Bmatrix} \frac{\partial f}{\partial x} \\ \frac{\partial f}{\partial y} \end{Bmatrix} = \begin{bmatrix} \frac{\partial \xi}{\partial x} & \frac{\partial \eta}{\partial x} \\ \frac{\partial \xi}{\partial y} & \frac{\partial \eta}{\partial y} \end{bmatrix} \begin{Bmatrix} \frac{\partial f}{\partial \xi} \\ \frac{\partial f}{\partial \eta} \end{Bmatrix} \quad (6.31)$$

If we consider two functions  $f_1 = x$  and  $f_2 = y$  then evaluation of (6.31) may be written in matrix form as

$$\begin{bmatrix} \frac{\partial f_1}{\partial x} & \frac{\partial f_2}{\partial x} \\ \frac{\partial f_1}{\partial y} & \frac{\partial f_2}{\partial y} \end{bmatrix} = \begin{bmatrix} 1 & 0 \\ 0 & 1 \end{bmatrix} = \begin{bmatrix} \frac{\partial \xi}{\partial x} & \frac{\partial \eta}{\partial x} \\ \frac{\partial \xi}{\partial y} & \frac{\partial \eta}{\partial y} \end{bmatrix} \begin{bmatrix} \frac{\partial x}{\partial \xi} & \frac{\partial y}{\partial \xi} \\ \frac{\partial x}{\partial \eta} & \frac{\partial y}{\partial \eta} \end{bmatrix} = \begin{bmatrix} \frac{\partial \xi}{\partial x} & \frac{\partial \eta}{\partial x} \\ \frac{\partial \xi}{\partial y} & \frac{\partial \eta}{\partial y} \end{bmatrix} \mathbf{J} \quad (6.32)$$

The array  $\mathbf{J}$  is known as the *Jacobian matrix* for the transformation and by the relation defining the parent coordinates [Eq. (6.19)], the matrix  $\mathbf{J}$  can be found explicitly in terms of the local coordinates.

To find now the global derivatives for  $f = N_a$  we invert  $\mathbf{J}$  and write (6.31) as

$$\begin{Bmatrix} \frac{\partial N_a}{\partial x} \\ \frac{\partial N_a}{\partial y} \end{Bmatrix} = \mathbf{J}^{-1} \begin{Bmatrix} \frac{\partial N_a}{\partial \xi} \\ \frac{\partial N_a}{\partial \eta} \end{Bmatrix} \quad (6.33)$$

In terms of the mapping defining the coordinate transformation we have

$$\mathbf{J} = \begin{bmatrix} \sum_a \frac{\partial N_a}{\partial \xi} x_a & \sum_a \frac{\partial N_a}{\partial \xi} y_a \\ \sum_a \frac{\partial N_a}{\partial \eta} x_a & \sum_a \frac{\partial N_a}{\partial \eta} y_a \end{bmatrix} \quad (6.34)$$

The inverse of the Jacobian matrix is easily obtained from (6.32) and is given by

$$\mathbf{J}^{-1} = \frac{1}{j} \begin{bmatrix} \frac{\partial y}{\partial \eta} & -\frac{\partial y}{\partial \xi} \\ -\frac{\partial x}{\partial \eta} & \frac{\partial x}{\partial \xi} \end{bmatrix} \quad (6.35a)$$

where

$$j = \det \mathbf{J} = \frac{\partial x}{\partial \xi} \frac{\partial y}{\partial \eta} - \frac{\partial x}{\partial \eta} \frac{\partial y}{\partial \xi} \quad (6.35b)$$

is the determinant of the Jacobian matrix.

For triangular elements it is necessary to modify the above since all the  $L_j$  are not independent but are constrained by their sum being unity. Thus, to compute the derivatives we now include the constraint as one of the functions to be differentiated and express derivatives as

$$\frac{\partial f}{\partial x} = \sum_{i=1}^3 \frac{\partial f}{\partial L_i} \frac{\partial L_i}{\partial x} \quad \text{and} \quad \frac{\partial f}{\partial y} = \sum_{i=1}^3 \frac{\partial f}{\partial L_i} \frac{\partial L_i}{\partial y} \quad (6.36)$$

The derivatives of the area coordinates now may be obtained by differentiating the three equations

$$\mathbf{f} = \begin{Bmatrix} 1 \\ x \\ y \end{Bmatrix} = \begin{Bmatrix} \sum_{i=1}^3 L_i \\ \sum_a N_a x_a \\ \sum_a N_a y_a \end{Bmatrix}$$

Using the chain rule, the derivatives of  $\mathbf{f}$  with respect to  $x$  and  $y$  now may be written as

$$\begin{bmatrix} 0 & 0 \\ 1 & 0 \\ 0 & 1 \end{bmatrix} = \begin{bmatrix} 1 & 1 & 1 \\ X_1 & X_2 & X_3 \\ Y_1 & Y_2 & Y_3 \end{bmatrix} \begin{bmatrix} \frac{\partial L_1}{\partial x} & \frac{\partial L_1}{\partial y} \\ \frac{\partial L_2}{\partial x} & \frac{\partial L_2}{\partial y} \\ \frac{\partial L_3}{\partial x} & \frac{\partial L_3}{\partial y} \end{bmatrix}$$

where we denote the parent derivatives by

$$X_i = \sum_a \frac{\partial N_a}{\partial L_i} x_a \quad \text{and} \quad Y_i = \sum_a \frac{\partial N_a}{\partial L_i} y_a$$

The solution yields

$$\begin{bmatrix} \frac{\partial L_1}{\partial x} & \frac{\partial L_1}{\partial y} \\ \frac{\partial L_2}{\partial x} & \frac{\partial L_2}{\partial y} \\ \frac{\partial L_3}{\partial x} & \frac{\partial L_3}{\partial y} \end{bmatrix} = \begin{bmatrix} 1 & 1 & 1 \\ X_1 & X_2 & X_3 \\ Y_1 & Y_2 & Y_3 \end{bmatrix}^{-1} \begin{bmatrix} 0 & 0 \\ 1 & 0 \\ 0 & 1 \end{bmatrix} = \frac{1}{2\Delta} \begin{bmatrix} B_1 & C_1 \\ B_2 & C_2 \\ B_3 & C_3 \end{bmatrix} \quad (6.37)$$

where

$$\begin{aligned} B_1 &= Y_2 - Y_3, & C_1 &= X_3 - X_2 \\ B_2 &= Y_3 - Y_1, & C_2 &= X_1 - X_3 \\ B_3 &= Y_1 - Y_2, & C_3 &= X_2 - X_1 \end{aligned} \quad (6.38)$$

and  $\Delta = (X_1 B_1 + X_2 B_2 + X_3 B_3)/2$  denotes the Jacobian transformation for a triangle when using quadrature to evaluate integrals. The reader should note the similarity to the results obtained when originally developing shape functions for the three-node triangle; however, the above result also holds for higher order interpolations.

### 6.7.1 Placement of element coordinates

As noted above the mapping of elements from parent to global coordinates must always be single valued. That is each point  $\xi_i$ <sup>1</sup> of the parent coordinates must map to one and only one global coordinate  $\mathbf{x}$ . The parametric map is controlled by the placement of nodal coordinates  $\mathbf{x}_a$  for each element. The constraint to maintain a one-to-one mapping is given by the Jacobian determinant computed by the chain rule of differentiation. Denoting the Jacobian as  $j(\xi_i)$  the requirement is

$$j(\xi_i) > 0 \quad \text{for all } \xi_i \quad (6.39)$$

<sup>1</sup>Where  $\xi_i$  denotes any of the parent coordinates considered above.

For the lowest order elements one can establish criteria to ensure that the constraint is satisfied everywhere in the element. However, as the order of elements increases it is more difficult to ensure such criteria. To enforce the constraint the following must be checked:

1. Placement of edge nodes to make  $j$  positive.
2. Placement of face nodes to make  $j$  positive.
3. Placement of internal node to make  $j$  positive.
4. All vertex angles are less than  $180^\circ$ .

Checking that the value of  $j(\xi)$  is positive at each node of an element is sufficient to ensure the above conditions are satisfied and, thus, the specified parametric mapping produces a valid element.

## 6.8 Numerical integration

Once the shape functions and derivatives are known, the final step requires the evaluation of integrals to obtain the element matrices.

### 6.8.1 Quadrilateral elements

While integrals for a rectangular four-node element may be quite easily obtained, the integration becomes much more difficult for axisymmetric and mapped elements using parent coordinates. Thus, in general, it is best to consider the use of quadrature (numerical integration) as a general computational tool.

Using the isoparametric concept it is first necessary to change the domain over which the elements are integrated. This is a standard operation the reader learned in integral calculus. Thus, for a two-dimensional problem using quadrilateral elements the integral over  $\Omega_e$  is converted to an integral over the parent domain  $-1 \leq \xi, \eta \leq 1$  as

$$\int_{\Omega_e} g(x, y) dx dy = \int_{-1}^1 \int_{-1}^1 \hat{g}(\xi, \eta) j(\xi, \eta) d\xi d\eta \quad (6.40)$$

where  $j(\xi, \eta)$  is the determinant of the Jacobian matrix described above. Using the isoparametric form the transformation of the integrand is accomplished as

$$g(x, y) = g(x(\xi, \eta), y(\xi, \eta)) = \hat{g}(\xi, \eta) \quad (6.41)$$

With the above choice for the domain of the parent element is now convenient to evaluate integrals using Gaussian quadrature as described in Section 3.5.3. Accordingly, we can integrate in two directions using

$$\int_{\Omega_e} g(x, y) dx dy = \sum_{n=1}^N \sum_{m=1}^M \hat{g}(\xi_m, \eta_n) j(\xi_m, \eta_n) w_m w_n + R_{NM} \quad (6.42)$$

where  $m$  denotes quadrature points in the  $\xi$  direction, and  $n$  quadrature points in the  $\eta$  direction.  $R_{NM}$  is a remainder term representing the difference between the exact

integral and the approximation by the sum at the quadrature points. When using quadrature one needs to be assured that sufficient points are used such that the remainder term is of the same order or less than the other errors in the solution procedure. This is considered further in Section 6.8.5. The location and weight for quadrature points in each direction are those given in Table 3.3 for one-dimensional integrations.

### 6.8.2 Brick elements

Integrals for brick elements are performed in a similar manner to that used for quadrilateral shapes. For a three-dimensional problem the quadrature over the domain  $\Omega_e$  is converted to an integral over the parent domain  $-1 \leq \xi, \eta, \zeta \leq 1$  as

$$\int_{\Omega_e} g(x, y, z) dx dy dz = \int_{-1}^1 \int_{-1}^1 \int_{-1}^1 \hat{g}(\xi, \eta, \zeta) j(\xi, \eta, \zeta) d\xi d\eta d\zeta \quad (6.43)$$

where  $j(\xi, \eta, \zeta)$  is the determinant of the Jacobian matrix for the three-dimensional brick. Again using the parametric form the transformation of the integrand is accomplished as

$$g(x, y) = g(x(\xi, \eta, \zeta), y(\xi, \eta, \zeta), z(\xi, \eta, \zeta)) = \hat{g}(\xi, \eta, \zeta) \quad (6.44)$$

Now three sums are required giving the numerical integration form

$$\int_{\Omega_e} g(x, y, z) dx dy dz = \sum_{l=1}^L \sum_{m=1}^M \sum_{n=1}^M \hat{g}(\xi_l, \eta_m, \zeta_n) j(\xi_l, \eta_m, \zeta_n) w_l w_m w_n + R_{LNM} \quad (6.45)$$

where  $l$  denotes quadrature points in the  $\xi$  direction,  $m$  quadrature points in the  $\eta$  direction, and  $n$  quadrature points in the  $\zeta$  direction.  $R_{LNM}$  is a remainder term representing the difference between the exact integral and the approximation by the sum at the quadrature points.

### 6.8.3 Triangular elements

For a triangle, in terms of the area coordinates the integrals are of the form

$$I = \int_0^1 \int_0^{1-L_1} f(L_1, L_2, L_3) dL_2 dL_1, \quad L_3 = 1 - L_1 - L_2 \quad (6.46)$$

It is useful to note the following exact integration expression for triangular elements with constant Jacobian  $j$ :

$$\iint_{\Delta} L_1^a L_2^b L_3^c dx dy = \frac{a! b! c!}{(a + b + c + 2)!} 2\Delta \quad (6.47)$$

where  $\Delta$  is the area of the triangle. However, for general shaped triangles it is again more convenient to use quadrature to evaluate integrals.

Once again we could use  $n$  Gauss points and arrive at a summation expression of the type used for quadrilaterals. However, the limits of integration now involve the variable itself and it is convenient to use alternative sampling points for the second integration by use of a special Gauss expression for integrals in which the integrand is multiplied by a linear function. These have been devised by Radau [18] and used successfully in the finite element context [19]. It is, however, much more desirable (and aesthetically pleasing) to use special formulae in which no bias is given to any of the natural coordinates  $L_a$ . Such formulae were first derived by Hammer et al. [20] and Felippa [21] and a series of necessary sampling points and weights is given in Table 6.3 [22–24].

#### 6.8.4 Tetrahedral elements

A similar extension for tetrahedra can obviously be made. For tetrahedral elements we note the exact integral expression is given for constant Jacobian elements by

$$\iiint_V L_1^a L_2^b L_3^c L_4^d dx dy dz = \frac{a! b! c! d!}{(a + b + c + d + 3)!} 6V \quad (6.48)$$

where  $V$  is the volume of the tetrahedron given in (5.24a). Similarly, Table 6.4 presents some quadrature formulae based on Ref. [20].

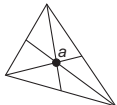
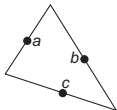
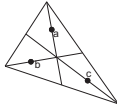
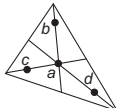
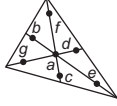
#### 6.8.5 Required order of numerical integration

At this point the reader may inquire as to how many points need to be used to evaluate the arrays. There are some basic rules that should not be violated, however, it is obvious that use of quadrature will imply that all integrals in the arrays may not be exactly computed. Since we have already introduced approximation into the solution process by using polynomial shape functions all that is required is that the quadrature errors be less than these discretization errors. In addition, we need to ensure that some basic physical and mathematical properties are preserved. It is of interest, therefore, to determine (a) the minimum integration requirement permitting convergence and (b) the integration requirements necessary to preserve the rate of convergence which would result if exact integration were used.

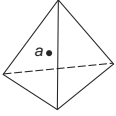
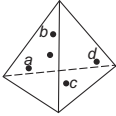
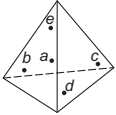
It will be found later (Chapters 8 and 10) that it is in fact often a disadvantage to use higher orders of integration than those actually needed under (b) as, for very good reasons, a “cancellation of errors” due to discretization and due to inexact integration can occur.

##### 6.8.5.1 Minimum order of integration for convergence

In problems where the variational functional (or equivalent Galerkin integral statements) defines the approximation we have already stated that convergence can occur providing any arbitrary constant value of  $m$ th derivatives can be reproduced. In the present  $C_0$  case  $m = 1$  and we thus require that in integrals of  $G^e$  a constant value be correctly integrated. *Thus the volume of the element  $\int_{\Omega} d\Omega$  needs to be evaluated correctly for convergence to occur.* In curvilinear coordinates we can thus argue that for a three-dimensional problem  $\int j(\xi, \eta, \zeta) d\xi d\eta d\zeta$  has to be evaluated exactly [25,26].

Table 6.3 Numerical Integration Formulae for Triangles						
Order	Figure	Error	Points	Triangular Coordinates	Weights	
Linear		$R = O(h^2)$	$a$	$\frac{1}{3}, \frac{1}{3}, \frac{1}{3}$	1	
Quadratic		$R = O(h^3)$	$a$	$\frac{1}{2}, \frac{1}{2}, 0$	$\frac{1}{3}$	
			$b$	$\frac{1}{2}, 0, \frac{1}{2}$	$\frac{1}{3}$	
			$c$	$0, \frac{1}{2}, \frac{1}{2}$	$\frac{1}{3}$	
Quadratic		$R = O(h^3)$	$a$	$\frac{2}{3}, \frac{1}{6}, \frac{1}{6}$	$\frac{1}{3}$	
			$b$	$\frac{1}{6}, \frac{2}{3}, \frac{1}{6}$	$\frac{1}{3}$	
			$c$	$\frac{1}{6}, \frac{1}{6}, \frac{2}{3}$	$\frac{1}{3}$	
Cubic		$R = O(h^4)$	$a$	$\frac{1}{3}, \frac{1}{3}, \frac{1}{3}$	$-\frac{27}{48}$	
			$b$	0.6, 0.2, 0.2	$\frac{25}{48}$	
			$c$	0.2, 0.6, 0.2	$\frac{25}{48}$	
			$d$	0.2, 0.2, 0.6	$\frac{25}{48}$	
Quintic		$R = O(h^6)$	$a$	$\frac{1}{3}, \frac{1}{3}, \frac{1}{3}$	0.2250000000	
			$b$	$\alpha_1, \beta_1, \beta_1$	0.1323941527	
			$c$	$\beta_1, \alpha_1, \beta_1$	0.1323941527	
			$d$	$\beta_1, \beta_1, \alpha_1$	0.1323941527	
			$e$	$\alpha_2, \beta_2, \beta_2$	0.1259391805	
			$f$	$\beta_2, \alpha_2, \beta_2$	0.1259391805	
			$g$	$\beta_2, \beta_2, \alpha_2$	0.1259391805	
with						
$\alpha_1 = 0.059\,715\,871\,7$						
$\beta_1 = 0.470\,142\,064\,1$						
$\alpha_2 = 0.797\,426\,985\,3$						
$\beta_2 = 0.101\,286\,507\,3$						

**Table 6.4** Numerical Integration Formulae for Tetrahedra

Order	Figure	Error	Points	Tetrahedral Coordinates	Weights
Linear		$R = O(h^2)$	$a$	$\frac{1}{4}, \frac{1}{4}, \frac{1}{4}, \frac{1}{4}$	1
Quadratic		$R = O(h^3)$	$a$	$\alpha, \beta, \beta, \beta$	$\frac{1}{4}$
			$b$	$\beta, \alpha, \beta, \beta$	$\frac{1}{4}$
			$c$	$\beta, \beta, \alpha, \beta$	$\frac{1}{4}$
			$d$	$\beta, \beta, \beta, \alpha$	$\frac{1}{4}$
			$\alpha = 0.585\,410\,20$ $\beta = 0.138\,196\,60$		
Cubic		$R = O(h^4)$	$a$	$\frac{1}{4}, \frac{1}{4}, \frac{1}{4}, \frac{1}{4}$	$-\frac{4}{5}$
			$b$	$\frac{1}{2}, \frac{1}{6}, \frac{1}{6}, \frac{1}{6}$	$\frac{9}{20}$
			$c$	$\frac{1}{6}, \frac{1}{2}, \frac{1}{6}, \frac{1}{6}$	$\frac{9}{20}$
			$d$	$\frac{1}{6}, \frac{1}{6}, \frac{1}{2}, \frac{1}{6}$	$\frac{9}{20}$
			$e$	$\frac{1}{6}, \frac{1}{6}, \frac{1}{6}, \frac{1}{2}$	$\frac{9}{20}$

**6.8.5.2 Order of integration for no loss of convergence rate**

In the one-dimensional problem we have already found that the finite element approximate evaluation of energy (and indeed all the other integrals in a Galerkin-type approximation, see Chapter 3) was exact to the order  $2(p - m)$ , where  $p$  is the degree of the complete polynomial present and  $m$  is the order of differential occurring in the appropriate expressions.

Providing the integration is exact to order  $2(p - m)$ , or shows an error of  $O(h^{2(p-m)+1})$ , or less, then no loss of convergence order will occur.<sup>2</sup> If in curvilinear

<sup>2</sup>For an energy principle use of quadrature may result in loss of a bound for  $\Pi(\tilde{\mathbf{u}})$ .



coordinates we take a curvilinear dimension  $h$  of an element, the same rule applies. For  $C_0$  problems (i.e.,  $m = 1$ ) the integration formulae should be as follows:

$$\begin{aligned} p = 1, & \quad \text{linear elements} & O(h) \\ p = 2, & \quad \text{quadratic elements} & O(h^3) \\ p = 3, & \quad \text{cubic elements} & O(h^5) \end{aligned}$$

We shall make use of these results in practice, as will be seen later, but it should be noted that for a linear quadrilateral or triangle a single-point integration is adequate. For parabolic quadrilaterals (or bricks)  $2 \times 2$  (or  $2 \times 2 \times 2$ ), Gauss point integration is adequate and for parabolic triangles (or tetrahedra) the three-point (and four-point) formulae of Tables 6.3 and 6.4 are needed.

The basic theorems of this section have been introduced and proved numerically in published work [27–29].

### 6.8.6 Matrix singularity due to numerical integration

The final outcome of a semi-discretized finite element approximation of the quasi-harmonic equation was

$$\mathbf{C}\dot{\tilde{\boldsymbol{\phi}}} + \mathbf{H}\tilde{\boldsymbol{\phi}} = \mathbf{s} \quad (6.49)$$

For the one-dimensional elasticity problem it was of the form

$$\mathbf{M}\ddot{\tilde{\mathbf{u}}} + \mathbf{K}\tilde{\mathbf{u}} = \mathbf{f} \quad (6.50)$$

which we will also find in higher dimensional problems in the next chapter. For steady-state, static problems the first term is omitted. In each, if required, boundary conditions have been inserted. The solution of (6.49) or (6.50) gives an approximate solution for the physical situation. If a solution is unique, as is the case with well-posed physical problems, the equation matrix  $\mathbf{C}$  or  $\mathbf{M}$  should be positive definite (have full rank). The equation matrix  $\mathbf{H}$  or  $\mathbf{K}$  should have proper rank and be positive semi-definite. The rank of a square symmetric matrix is determined from an eigen-problem of the form

$$\mathbf{A}\boldsymbol{\Phi} = \boldsymbol{\Phi}\boldsymbol{\Lambda}$$

where  $\boldsymbol{\Lambda}$  is a diagonal matrix of eigenvalues and  $\boldsymbol{\Phi}$  is a square matrix whose columns are the eigenvectors (see Appendix A). The rank of the matrix is the number of nonzero eigenvalues. If all eigenvalues are positive a matrix is positive definite; if all are positive or zero the matrix is positive semi-definite. Applying to (6.49), for the quasi-harmonic equation  $\mathbf{C}$  should have rank  $n - 1$  where  $n$  is the size of the matrix without any boundary conditions. This implies the need for one boundary condition of the type  $\phi_a = \bar{\phi}_a$  on one node. For elasticity  $\mathbf{K}$  can admit rigid body modes only and we shall address this further in the next chapter.

We have *a priori* assumed that these conditions are satisfied with exact integration. With numerical integration, singularities may arise for low integration orders, and this may make such orders impractical. It is easy to show how, in some circumstances, a

singularity of a matrix must arise, but it is more difficult to prove that it will not. We shall, therefore, concentrate on the former case.

With numerical integration we replace the integrals by a weighted sum of independent linear relations between the nodal parameters (e.g.,  $\tilde{\phi}$  for the quasi-harmonic equation). These linear relations supply the only information from which the matrices  $\mathbf{H}$  and  $\mathbf{C}$  are constructed. *If the number of unknowns exceeds the number of independent relations supplied at all the integrating points, then the matrix must be singular.*

To illustrate this point consider a two-dimensional quasi-harmonic problem where the evaluation of the element matrices by numerical integration may be written as

$$\mathbf{C}^e = \sum_{l=1}^L \mathbf{N}(\xi_l)^T c(\xi_l) \mathbf{N}(\xi_l) j(\xi_l) W_l$$

$$\mathbf{H}^e = \sum_{l=1}^L \mathbf{b}(\xi_l)^T \mathbf{k}(\xi_l) \mathbf{b}(\xi_l) j(\xi_l) W_l$$

where  $L$  denotes the total number of quadrature points and  $\xi_l$  the appropriate points (e.g.,  $\xi$  or  $L_1$ , etc.). In the above, each matrix is evaluated at quadrature point  $l$  and has the form

$$\mathbf{N}(\xi_l) = [N_1 \ N_2 \ \cdots \ N_n]_{\xi_l}$$

$$\mathbf{b}(\xi_l) = \begin{bmatrix} \frac{\partial N_1}{\partial x} & \frac{\partial N_2}{\partial x} & \cdots & \frac{\partial N_n}{\partial x} \\ \frac{\partial N_1}{\partial y} & \frac{\partial N_2}{\partial y} & \cdots & \frac{\partial N_n}{\partial y} \end{bmatrix}_{\xi_l}$$

$$\mathbf{k}(\xi_l) = \begin{bmatrix} k_{xx} & k_{xy} \\ k_{yx} & k_{yy} \end{bmatrix}_{\xi_l}$$

where  $n$  is the number of nodes on an individual element. The quadrature sum for each element array also may be written in the matrix form

$$\mathbf{C}^e = [\mathbf{N}^T(\xi_1) \ \mathbf{N}^T(\xi_2) \ \cdots \ \mathbf{N}^T(\xi_L)] \begin{bmatrix} \widehat{c}(\xi_1) & & & \\ & \widehat{c}(\xi_2) & & \\ & & \ddots & \\ & & & \widehat{c}(\xi_L) \end{bmatrix} \begin{bmatrix} \mathbf{N}(\xi_1) \\ \mathbf{N}(\xi_2) \\ \vdots \\ \mathbf{N}(\xi_L) \end{bmatrix}$$

$$\mathbf{H}^e = [\mathbf{b}^T(\xi_1) \ \mathbf{b}^T(\xi_2) \ \cdots \ \mathbf{b}^T(\xi_L)] \begin{bmatrix} \widehat{\mathbf{k}}(\xi_1) & & & \\ & \widehat{\mathbf{k}}(\xi_2) & & \\ & & \ddots & \\ & & & \widehat{\mathbf{k}}(\xi_L) \end{bmatrix} \begin{bmatrix} \mathbf{b}(\xi_1) \\ \mathbf{b}(\xi_2) \\ \vdots \\ \mathbf{b}(\xi_L) \end{bmatrix}$$

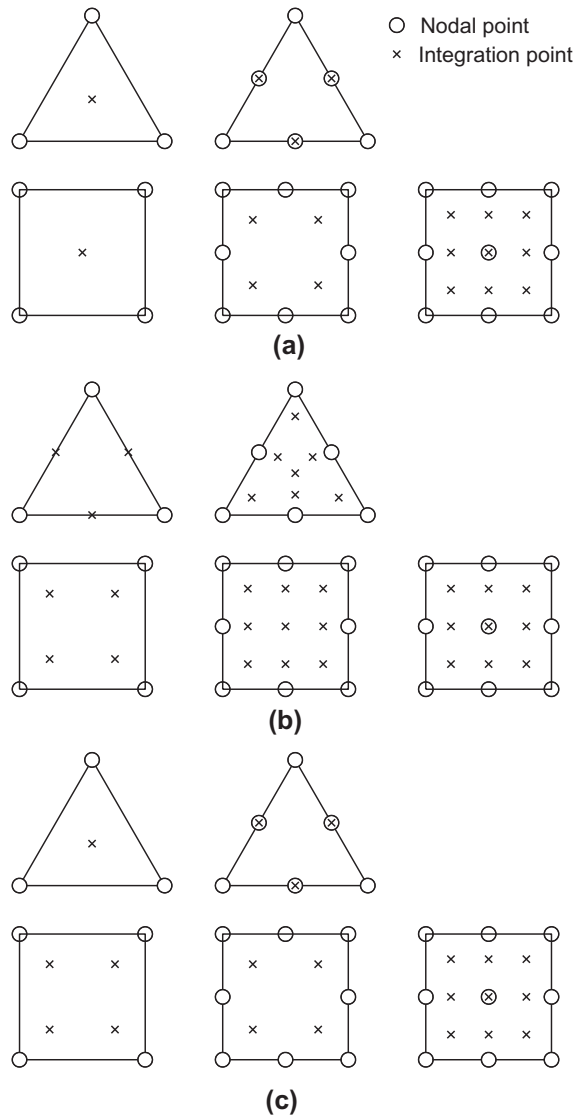
where

$$\widehat{c}(\xi_l) = c(\xi_l) j(\xi_l) W_l \quad \text{and} \quad \widehat{\mathbf{k}}(\xi_l) = \mathbf{k}(\xi_l) j(\xi_l) W_l$$

The rank of a nonsquare matrix is equal to or less than its smaller dimension. Also in estimating rank any row or column of all zeros is ignored. In the above the rank of  $\mathbf{N}(\xi_I)$  and  $\hat{\mathbf{c}}(\xi_I)$  is 1. Similarly, the rank of  $\mathbf{b}(\xi_I)$  and  $\mathbf{k}(\xi_I)$  is 2. For each quadrature point the rank of the resulting matrix products is the minimum of the rank of the contributing matrices. In accumulating quadrature points the rank may increase by the rank of each point, however, it will eventually reach a maximum due to linear dependence between the individual contributions and become the rank of the columns of the  $\mathbf{N}$  and  $\mathbf{b}$  matrices. For the quasi-harmonic equation the column rank of the  $\mathbf{N}$  matrices is  $n$ , the number of element nodes. For any set of element shape functions which satisfy  $\sum_{a=1}^n N_a(\xi) = 1$  the sum of any existing derivatives can always be zero. Thus, the column rank of the  $\mathbf{b}$  matrix will be  $n - 1$ , indicating the available “rigid body mode” in  $\mathbf{C}^e$ . Thus, at some number of  $L$  the rank of the resulting matrix does not change with increasing number of points; only the accuracy of computed terms may change. Indeed, only in cases where all terms in the matrices are of polynomial form can the exact value (to within computer round-off) of an integral be computed (i.e., the remainder is zero in the quadrature formula) using the formulae given above and in Chapter 3.

Based on the above we can now estimate the number of points needed to compute the  $\mathbf{C}^e$  and  $\mathbf{H}^e$  matrices for the quasi-harmonic equation. For comparison we consider three- and six-node triangular elements and four-, eight-, and nine-node quadrilateral elements. For the elements considered, the computation of  $\mathbf{C}^e$  requires at least one quadrature point for each element node. At each integrating point *two* independent “gradient relations” are used to compute  $\mathbf{H}^e$  and the total number of independent relations possibly equals  $2 \times (\text{number of integration points})$ . Since a constant value of  $\phi$  does not change a derivative, the required rank for  $\mathbf{C}^e$  is 1 less than the number of element nodes. Thus, we estimate that a single quadrature point can be used for the three-node element and three points can be used for the six-node element. For the quadrilateral element the estimate is two points for the four-node element, four points for the eight-node element, and five points for the nine-node element. Of course, suitable points need to exist. At present we have only identified use of one-dimensional Gaussian quadrature for each direction of quadrilaterals and brick elements, thus, for these the minimum estimates would use  $2 \times 2$  quadrature ( $L = 4$ ) for the four- and eight-node elements and  $3 \times 3$  quadrature ( $L = 9$ ) for the nine-node element. The above choices are shown in Fig. 6.22. *We emphasize that the above are merely estimates.* When computing an element by numerical integration it is always important to check individual element arrays to ensure they have proper rank.

The above results indicate that often different order quadrature is required in order to attain proper rank of the  $\mathbf{C}^e$  and  $\mathbf{H}^e$  matrices. In the above we have emphasized both rank and accuracy and we note that it is possible in low order elements to obtain sufficient accuracy before proper rank is obtained. We shall refer to the minimum value of  $L$  that gives full rank as *normal order quadrature* and a value of  $L - 1$  as *reduced quadrature*. There are instances when reduced quadrature has been used,

**FIGURE 6.22**

Required quadrature for two-dimensional quasi-harmonic problems: (a) exact Jacobian, (b)  $\mathbf{C}^e$  (mass) matrix, and (c)  $\mathbf{H}^e$  (stiffness) matrix.

for instance, it is commonly used in “explicit” dynamics codes—but requires certain remedial additions (e.g., hourglass control [30,31]).

In Chapter 8 we shall return to the problem of convergence and will indicate dangers arising from local element singularities.

However, it is of interest to mention that in Chapter 10 we shall in fact *seek* matrix singularities for special purposes (e.g., elastic incompressibility) using similar arguments.

## 6.9 Shape functions by degeneration

In the previous sections we have discussed the construction of shape functions for mapped elements of Lagrangian and serendipity types, as well as those for triangular and tetrahedral types. We have also shown how mixtures of interpolation forms may be used to construct elements of the prism type. One may ask what happens if we distort elements such that nodes for the Lagrangian or serendipity type are coalesced—that is, they are assigned the same node number in the mesh. We call the approach where two or more nodes are common a *degenerate form*. In a degenerate form the shape function for a coalesced set of two or more nodes is obtained by combining together the shape functions of sets of nodes (in a hierarchic form, any mid-side and/or face functions are omitted).

### Example 6.1. Four-Node quadrilateral degenerated into a triangle

As a simple example we consider the degeneration of a four-node quadrilateral in which nodes 3 and 4 are coalesced to form the third node of a triangular element as shown in Fig. 6.23. For an isoparametric form given in  $\xi, \eta$  coordinates, the shape functions for the degenerate triangular element are given by

$$\begin{aligned} N_1 &= \frac{1}{4}(1 - \xi)(1 - \eta) \\ N_2 &= \frac{1}{4}(1 + \xi)(1 - \eta) \\ N_3 &= \frac{1}{2}(1 + \eta) \end{aligned} \quad (6.51)$$

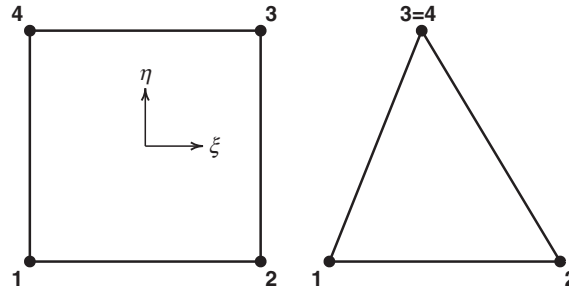


**FIGURE 6.23**

Degeneration of a quadrilateral into a triangle.

where the last function results from adding together the standard shape functions for nodes 3 and 4 of the quadrilateral element. Computing now the global derivatives for the above functions we obtain [using (6.31)]

$$\frac{\partial N_a}{\partial x} = \frac{b_a(1-\eta)}{2\Delta(1-\eta)}, \quad \frac{\partial N_a}{\partial y} = \frac{c_a(1-\eta)}{2\Delta(1-\eta)} \quad (6.52)$$

where  $b_a$  and  $c_a$  coincide with results for the standard three-node triangular element shape functions given in Section 6.2.1.1. Except for the point  $\eta = 1$  (the point where the nodes are coalesced) the shape function derivatives are constant and identical to those obtained using area coordinates  $L_1, L_2, L_3$ . Thus, for the degeneration we have the identities

$$\begin{aligned} N_1 &= \frac{1}{4}(1-\xi)(1-\eta) = L_1 \\ N_2 &= \frac{1}{4}(1+\xi)(1-\eta) = L_2 \\ N_3 &= \frac{1}{2}(1+\eta) = L_3 \end{aligned} \quad (6.53)$$

and, provided we do not consider the point  $\eta = 1$ , we may compute the derivatives and integrals for three-node triangular elements using the degeneration process.

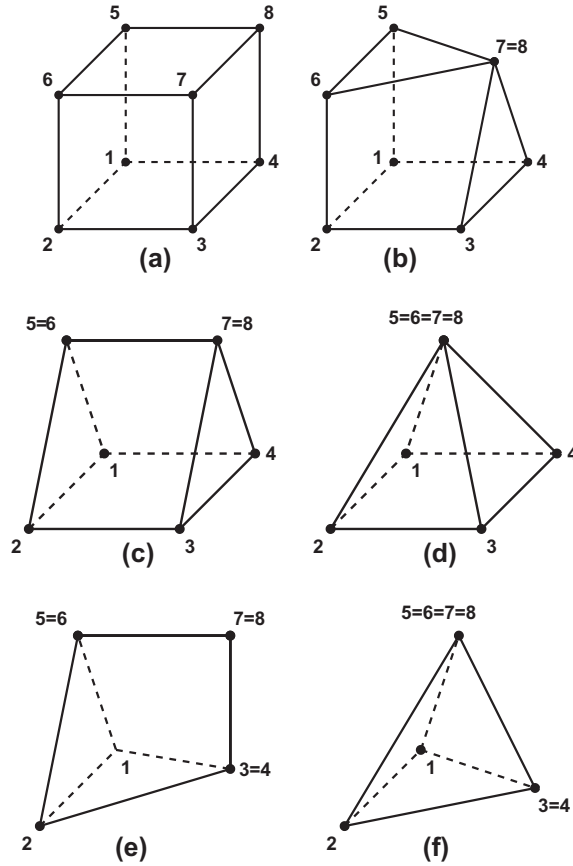
A similar form to the above example holds when an eight-node brick element is degenerated into a four-node tetrahedron. In addition, however, we can compute shape functions for other degenerate forms as indicated in Fig. 6.24. In all cases, the computation of derivatives gives a 0/0 form at any point where nodes are coalesced. In addition, however, any faces which degenerate into an edge will also contain a 0/0 in the derivative along that edge. The behavior on any remaining face of a degenerate element is either the original quadrilateral one or a triangular one in which the shape functions are identical to the results given in (6.53).

### 6.9.1 Higher order degenerate elements

When nodes for higher order quadrilateral and hexahedral elements are coalesced to give a degenerate form, it is necessary to modify the shape functions for some of the noncoalesced nodes in order to produce results which are consistent with those computed using area or volume coordinates, respectively. This aspect was first studied by Newton [32] and Irons [33] for serendipity-type elements. Here we extend the work reported in these references to include the Lagrangian-type elements. Using Lagrangian elements has a distinct advantage since all the degenerate elements preserve the properties of higher order approximation in global coordinates when the element is mapped according to the trilinear form (i.e., a sub-parametric form using the eight-node hexahedron) (see Fig. 6.25).

**Example 6.2.** Quadratic quadrilateral degenerated to a triangular element

As an example we consider the degeneration of a quadratic order quadrilateral to form a quadratic order triangular element. Expressing the shape functions in hierarchical

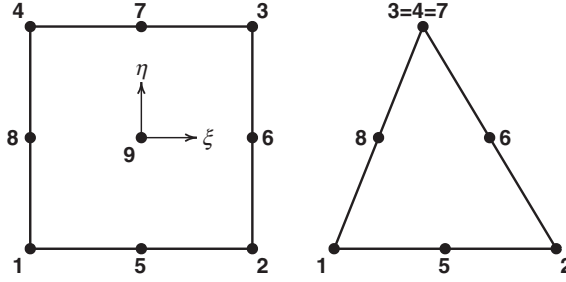
**FIGURE 6.24**

Some degenerate element forms for an eight-node brick element: (a) brick, (b) degenerate, (c) prism, (d) pyramid, (e) chisel, and (f) tetrahedron.

form (viz. Section 3.6) we have for the eight- or nine-node quadrilateral<sup>3</sup>

$$\begin{aligned}
 N_a^Q &= \frac{1}{4}(1 + \xi_a \xi)(1 + \eta_a \eta), \quad a = 1, 2, 3, 4 \\
 N_a^Q &= \frac{1}{2}(1 + \eta_a \eta)(1 - \xi^2), \quad a = 5, 7 \\
 N_a^Q &= \frac{1}{2}(1 + \xi_a \xi)(1 - \eta^2), \quad a = 6, 8 \\
 N_a^Q &= (1 - \xi^2)(1 - \eta^2), \quad a = 9
 \end{aligned} \tag{6.54}$$

<sup>3</sup>We use a superscript “ $Q$ ” for shape functions associated with the quadrilateral form and, later, “ $T$ ” to denote those for a triangular form.

**FIGURE 6.25**

Degeneration of a eight- or nine-node quadrilateral into a six-node triangle.

for which a hierarchical Lagrangian interpolation of any function is given by

$$f = \sum_{a=1}^4 N_a^Q(\xi, \eta) f_a + \sum_{a=5}^8 N_a^Q(\xi, \eta) \Delta f_a + N_9^Q(\xi, \eta) \Delta \Delta f_9 \quad (6.55)$$

where  $f_a$  are nodal values,  $\Delta f_a$  are departures from linear interpolation for mid-side nodes, and  $\Delta \Delta f_9$  is the departure from the eight-node serendipity interpolation at the center node. Thus, omitting the ninth function gives the serendipity form. If we now coalesce the nodes 3, 4, and 7 and use the above hierarchic form, the shape functions for the vertex nodes again are given by

$$\begin{aligned} N_1^Q &= \frac{1}{4}(1 - \xi)(1 - \eta) = L_1 = N_1^T \\ N_2^Q &= \frac{1}{4}(1 + \xi)(1 - \eta) = L_2 = N_2^T \\ N_3^Q &= \frac{1}{2}(1 + \eta) = L_3 = N_3^T \end{aligned} \quad (6.56)$$

(Note that  $\Delta f_7 = 0$  in any interpolation and, thus,  $N_7^T = 0$ .) Also, for the six-node form we omit the interior node 9 and thus, for the degenerate element  $N_9^T = 0$ . If the resulting degenerate element is to be identical with the six-node triangular element we require

$$\begin{aligned} N_5^T &= 4 L_1 L_2 \\ N_6^T &= 4 L_2 L_3 \\ N_8^T &= 4 L_3 L_1 \end{aligned} \quad (6.57)$$



Substituting the definitions for area coordinates given by (6.56) into (6.57) we find

$$\begin{aligned} N_5^T &= \frac{1}{4}(1 - \xi^2)(1 - \eta)^2 \\ N_6^T &= \frac{1}{2}(1 + \xi)(1 - \eta^2) \\ N_8^T &= \frac{1}{2}(1 - \xi)(1 - \eta^2) \end{aligned} \quad (6.58)$$

and, thus, comparing the forms given by (6.55) and (6.58) we obtain the result

$$N_5^T \neq N_5^Q, \quad N_6^T = N_6^Q, \quad N_8^T = N_8^Q \quad (6.59)$$

Thus, it only remains to correct the shape function for node 5. This is accomplished by noting

$$\begin{aligned} N_5^T &= \frac{1}{4}(1 - \xi^2)(1 - 2\eta + \eta^2) \\ &= \frac{1}{4}(1 - \xi^2)(2 - 2\eta - 1 + \eta^2) \\ &= \frac{1}{2}(1 - \xi^2)(1 - \eta) - \frac{1}{4}(1 - \xi^2)(1 - \eta^2) \end{aligned}$$

giving the “corrected” degenerate function for node 5 as

$$N_5^T = N_5^Q - \frac{1}{4}N_9^Q \quad (6.60)$$

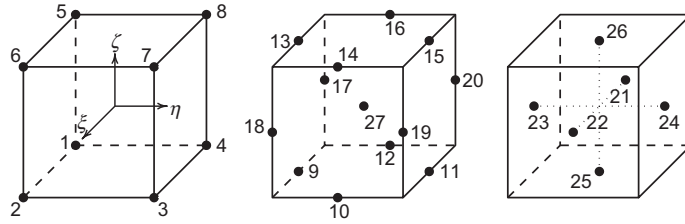
The hierarchical forms now can be converted to standard isoparametric form using the process given for serendipity elements in Section 6.2.2.4.

**Example 6.3.** Degenerate forms for a quadratic 27-node hexahedron

The construction for quadratic degenerate three-dimensional forms follows a similar process and, when using the hierarchical form, the mid-side node opposite each coalesced node on a “face” must be modified using a form similar to (6.60). Again, all the shapes shown in Fig. 6.24 are possible and permit the construction of meshes which can use a mix of bricks, tetrahedra, and degenerate transition forms. In addition to the 8 vertex nodes it is necessary to add 12 mid-edge nodes, 6 mid-face nodes, and 1 internal node to form a Lagrangian quadratic order hexahedron. For node numbers as given in Fig. 6.26 and using hierarchical interpolation, the shape functions are given by the following:

1. For vertex nodes:

$$N_a = \frac{1}{8}(1 + \xi_a \xi)(1 + \eta_a \eta)(1 + \zeta_a \zeta), \quad a = 1, 2, \dots, 8 \quad (6.61a)$$

**FIGURE 6.26**

Numbering for 27-node quadratic Lagrangian hexagon (node 27 at origin of  $\xi, \eta, \zeta$  coordinates).

2. For mid-edge nodes:

$$N_a = \frac{1}{4} \begin{cases} (1 - \xi^2)(1 + \eta_a \eta)(1 + \zeta_a \zeta), & a = 9, 11, 13, 15 \\ (1 + \xi_a \xi)(1 - \eta^2)(1 + \zeta_a \zeta), & a = 10, 12, 14, 16 \\ (1 + \xi_a \xi)(1 + \eta_a \eta)(1 - \zeta^2), & a = 17, 18, 19, 20 \end{cases} \quad (6.61b)$$

3. For mid-face nodes:

$$N_a = \frac{1}{2} \begin{cases} (1 + \xi_a \xi)(1 - \eta^2)(1 - \zeta^2), & a = 21, 22 \\ (1 - \xi^2)(1 + \eta_a \eta)(1 - \zeta^2), & a = 23, 24 \\ (1 - \xi^2)(1 - \eta^2)(1 + \zeta_a \zeta), & a = 25, 26 \end{cases} \quad (6.61c)$$

4. For the interior node:

$$N_a = (1 - \xi^2)(1 - \eta^2)(1 - \zeta^2), \quad a = 27 \quad (6.61d)$$

Table 6.5 indicates which shape functions are modified when vertex nodes are coalesced. The hierarchical shape functions to be omitted are also indicated. Note that shape functions should only be omitted (set to zero) after all coalesced node pairs are considered. Also if a tetrahedral element is formed then all mid-face nodes are deleted and the interior node may also be omitted, giving the final tetrahedron as a 10-node element. Again, if any of the element forms is mapped using the degenerate sub-parametric form of the eight-node hexahedron for  $N'_a$  full quadratic behavior in global coordinates is attained—showing the advantage of starting from Lagrangian form elements.

Consideration of cubic and higher order forms is also possible and is left as an exercise for the interested reader.

## 6.10 Generation of finite element meshes by mapping

It will be observed that it is an easy matter to obtain a coarse subdivision of the analysis domain with a small number of isoparametric elements. If second- or third-degree

elements are used, the fit of these to quite complex boundaries is reasonable, as shown in Fig. 6.27a where three parabolic elements specify a sectorial region. This number of elements would be too small for analysis purposes *but a simple subdivision into finer elements* can be done automatically using increments of the parent coordinates to define new element nodes and boundaries. The process thus allows us, with a small amount of original *input data*, to derive a finite element mesh of any refinement desirable. In Ref. [34] this type of mesh generation is developed for two- and three-dimensional solids and surfaces and is reasonably efficient. However, elements of predetermined size and/or gradation cannot be easily generated.

The main drawback of the mapping and generation suggested is the fact that the originally circular boundaries in Fig. 6.27a are approximated by simple parabolas and a geometric error can be developed there. To overcome this difficulty other forms of mapping can be adopted for this purpose.

An early form of mapping is the use of blending functions, originally developed for the representation of complex motor-car body shapes [35]. A simple use of blending functions is demonstrated in Fig. 6.27b to define the region with exact circular arcs instead of the parabolic ones from serendipity elements. These may be similarly subdivided to create the mesh shown in Fig. 6.27c.

### 6.10.1 Blending functions

Blending functions interpolate the unknown  $\phi$  in such a way as to satisfy *exactly* its variations along the edges of a square  $\xi, \eta$  domain. If the coordinates  $x$  and  $y$  are used in a parametric expression of the type given in Eq. (6.19), then any complex shape can be mapped by a single element. In Ref. [35] the region of Fig. 6.27 is in fact so mapped and a mesh subdivision obtained directly without any geometric error on the boundary.

**Table 6.5** Degeneration Modifications for 27-Node Hexahedron

Coalesced Nodes	Modified Nodes	
1 and 2 omit 9	11 by 25 omit 25	13 by 23 omit 23
2 and 3 omit 10	12 by 25 omit 25	14 by 22 omit 22
3 and 4 omit 11	9 by 25 omit 25	15 by 24 omit 24
4 and 1 omit 12	10 by 25 omit 25	16 by 21 omit 21
5 and 6 omit 13	15 by 26 omit 26	9 by 23 omit 23
6 and 7 omit 14	16 by 26 omit 26	10 by 22 omit 22
7 and 8 omit 15	13 by 26 omit 26	11 by 24 omit 24
8 and 5 omit 16	14 by 26 omit 26	12 by 21 omit 21
1 and 5 omit 17	18 by 23 omit 23	20 by 21 omit 21
2 and 6 omit 18	19 by 22 omit 22	17 by 23 omit 23
3 and 7 omit 19	20 by 24 omit 24	18 by 22 omit 22
4 and 8 omit 20	17 by 21 omit 21	19 by 24 omit 24

The blending processes are of considerable importance and have been used to construct some interesting element families [36] (which in fact include the standard serendipity elements as a subclass). To explain the process we shall show how a function with prescribed variations along the boundaries can be interpolated.

Consider a region  $-1 \leq \xi, \eta \leq 1$ , shown in Fig. 6.28, on the edges of which an arbitrary function  $\phi$  is specified [i.e.,  $\phi(-1, \eta)$ ,  $\phi(1, \eta)$ ,  $\phi(\xi, -1)$ ,  $\phi(\xi, 1)$  are given]. The problem presented is that of interpolating a function  $\phi(\xi, \eta)$  so that a smooth surface reproducing precisely the boundary values is obtained. Writing

$$\begin{aligned} N_1(\xi) &= \frac{1}{2}(1 - \xi), & N_2(\xi) &= \frac{1}{2}(1 + \xi) \\ N_1(\eta) &= \frac{1}{2}(1 - \eta), & N_2(\eta) &= \frac{1}{2}(1 + \eta) \end{aligned} \quad (6.62)$$

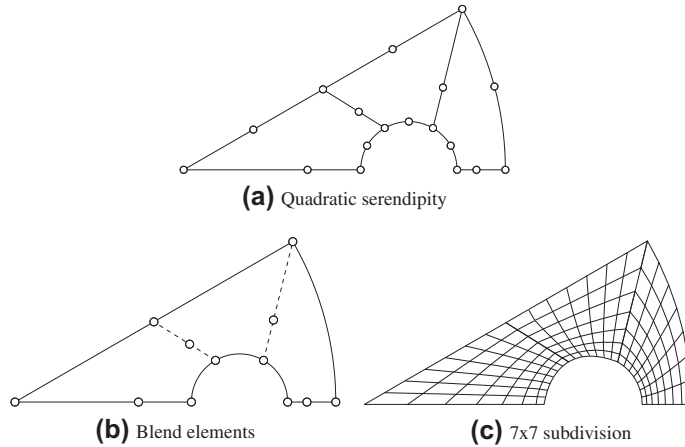
for our usual one-dimensional linear interpolating functions, we note that

$$P_\eta \phi \equiv N_1(\eta)\phi(\xi, -1) + N_2(\eta)\phi(\xi, 1) \quad (6.63)$$

interpolates linearly between the specified functions in the  $\eta$  direction, as shown in Fig. 6.28b. Similarly,

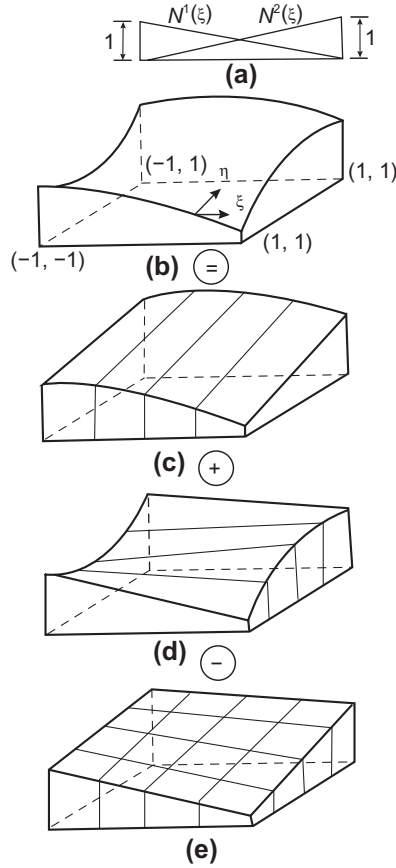
$$P_\xi \phi \equiv N_1(\xi)\phi(-1, \eta) + N_2(\xi)\phi(1, \eta) \quad (6.64)$$

interpolates linearly in the  $\xi$  direction (Fig. 6.28c). Constructing a third function which is a standard bilinear interpolation of the kind we have already encountered



**FIGURE 6.27**

Mesh generation by quadratic isoparametric elements: (a) quadratic serendipity element, (b) specified blending points, and (c) automatic subdivision into linear quadrilaterals.

**FIGURE 6.28**

Stages of construction of a blending interpolation (a)–(e).

(Fig. 6.28d), i.e.,

$$P_{\xi} P_{\eta} \phi = N_1(\xi) N_1(\eta) \phi(-1, -1) + N_1(\xi) N_2(\eta) \phi(-1, 1) + N_2(\xi) N_1(\eta) \phi(1, -1) + N_2(\xi) N_2(\eta) \phi(1, 1) \quad (6.65)$$

we note by inspection that

$$\phi(\xi, \eta) = P_{\eta} \phi + P_{\xi} \phi - P_{\xi} P_{\eta} \phi \quad (6.66)$$

is a smooth surface interpolating exactly the boundary functions.

Extension to functions with higher order blending is almost evident, and immediately the method of mapping the quadrilateral region  $-1 \leq \xi, \eta \leq 1$  to any arbitrary shape is obvious.

Though the above mesh generation method derives from mapping and indeed has been widely applied in two and three dimensions, we shall see in the chapter devoted to adaptivity (Chapter 16) that the optimal solution or specification of *mesh density* or *size* should guide the mesh generation. In Chapter 17 we will discuss in much more detail how meshes with prescribed density can be generated.

### 6.10.2 Bèzier functions

For simple shapes an alternative parameterization of the mapping function that also permits specification of many geometric shapes is the use of Bèzier functions. On the line defined by parent coordinate  $-1 \leq \xi \leq 1$ , the  $p$ th order Bèzier shape functions are given by the Bernstein polynomials [37]

$$B_{a+1}^{(p)}(\xi) = \frac{p!}{2^p a!(p-a)!} (1+\xi)^a (1-\xi)^{p-a}, \quad a = 0, 1, \dots, p \quad (6.67)$$

The end points for a Bèzier interpolation are associated with the points 1 and  $p+1$ . For the linear case  $p = 1$  and the two functions are given by

$$B_1^{(1)}(\xi) = \frac{1}{2}(1-\xi) \quad \text{and} \quad B_2^{(1)}(\xi) = \frac{1}{2}(1+\xi) \quad (6.68a)$$

These are identical to linear Lagrange interpolation. The quadratic order functions are given by

$$\begin{aligned} B_1^{(2)}(\xi) &= \frac{1}{4}(1-\xi)^2 \\ B_2^{(2)}(\xi) &= \frac{1}{2}(1-\xi)(1+\xi) \\ B_3^{(2)}(\xi) &= \frac{1}{4}(1+\xi)^2 \end{aligned} \quad (6.68b)$$

and shown in Fig. 6.29.

Bèzier shape functions satisfy the usual condition

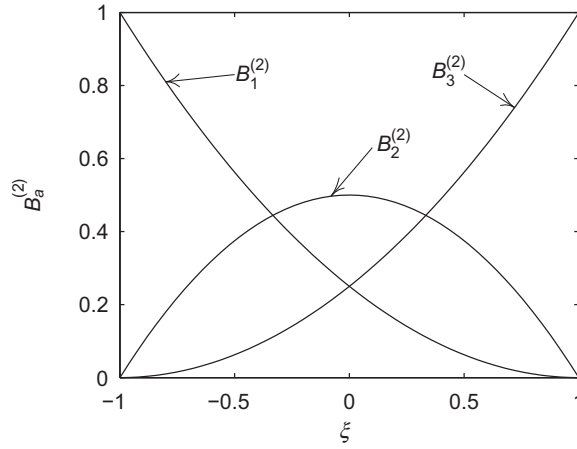
$$\sum_a B_a^{(p)}(\xi) = 1 \quad (6.69)$$

however, when used to describe the coordinates

$$\mathbf{x} = \sum_a B_a^{(p)}(\xi) \tilde{\mathbf{x}}_a \quad (6.70)$$

the curve does not pass through all the  $\tilde{\mathbf{x}}_a$  points. The  $\tilde{\mathbf{x}}_a$  are called the *control points* and define the geometry of any curve. This is illustrated in Fig. 6.30 as the parabola. It is also possible to modify the functions to a rational form as

$$R_a^{(p)}(\xi) = \frac{w_a B_a^{(p)}(\xi)}{w(\xi)} \quad (6.71a)$$

**FIGURE 6.29**

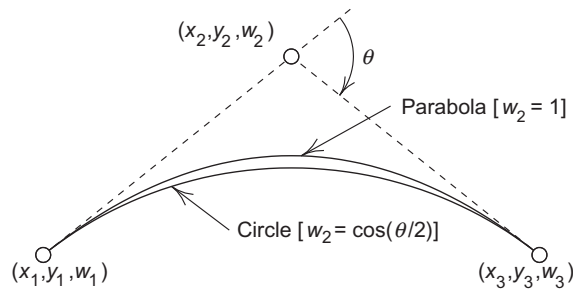
Quadratic Bèzier shape functions.

where

$$w(\xi) = \sum_a B_a^{(p)}(\xi) w_a \quad (6.71b)$$

defines a projective coordinate. The end values of  $w_a$  are always set to unity to ensure a function interpolates the end points. In the rational form it is possible to create an infinite number of curves by varying the value for the interior  $w_a$ . For example, a circular arc may be created using the quadratic functions by setting  $w_3 = \cos(\theta)$  as shown in Fig. 6.30. Setting all the  $w_a$  to unity recovers

$$R_a^{(p)}(\xi) = B_a^{(p)}(\xi)$$

**FIGURE 6.30**

Bèzier curves: parabola  $w_3 = 1$ ; circular arc  $w_3 = \cos(\theta)$ .

Two- and three-dimensional geometry may be created by using tensor products of the one-dimensional rational Bèzier functions. Thus, for two-dimensional surfaces one can use the form

$$\mathbf{x} = \sum_a \sum_b R_a^{(p)}(\xi) R_b^{(q)}(\eta) \tilde{\mathbf{x}}_{ab} \quad (6.72a)$$

and for three dimensions the form

$$\mathbf{x} = \sum_a \sum_b \sum_c R_a^{(p)}(\xi) R_b^{(q)}(\eta) R_c^{(r)}(\zeta) \tilde{\mathbf{x}}_{abc} \quad (6.72b)$$

may be used. Use of these permits the geometry of conic sections to be exactly matched over each Bèzier patch.

Bèzier functions can also be used to define elements, however, to retain a complete linear polynomial in the dependent variable it is necessary to use Bèzier functions for the coordinates also.

The use of the rational form for shape functions may be extended further to create *non-uniform rational B-splines* (NURBS) [37–39]. NURBS are commonly used by many computer-aided design (CAD) systems to create geometric models of physical entities. The output from a CAD system is usually not in a form that can be directly used for analysis. Often features of the design that do not affect analysis results need to be modified or removed. Once the model is in a form for analysis purposes, a “mesh” of nodes and elements must be created. The output of this step gives the finite element mesh for analysis and is followed by additional steps to assign appropriate boundary and initial conditions.

---

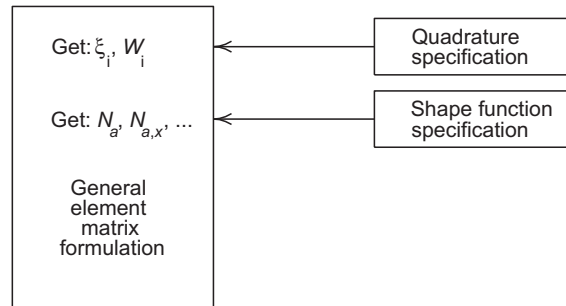
## 6.11 Computational advantage of numerically integrated finite elements

One considerable gain that is possible in numerically integrated finite elements is the versatility that can be achieved in a single computer program [40]. It will be observed that for a *given class of problems* the general matrices are always of the same form [see the example of Eq. (5.16)] in terms of the shape function and its derivatives.

To proceed with evaluation of the element properties it is necessary first to *specify the shape function* and its derivatives and, second, to *specify the order of integration*. The computation of element properties is thus composed of three distinct parts as shown in Fig. 6.31. For a *given class of problems* it is only necessary to change the prescription of the shape functions to achieve a variety of possible elements. Conversely, the *same shape function* routines can be used in many different classes of problem.

Use of different elements, testing the efficiency of a new element in a given context, or extension of programs to deal with new situations can thus be readily achieved, and considerable algebra avoided (with its inherent possibilities of mistakes). The



**FIGURE 6.31**

Computational scheme for numerically integrated elements ( $N_{a,x} = \partial N_a / \partial x$ ).

computer is thus placed in the position it deserves, i.e., of being the obedient slave capable of saving routine work.

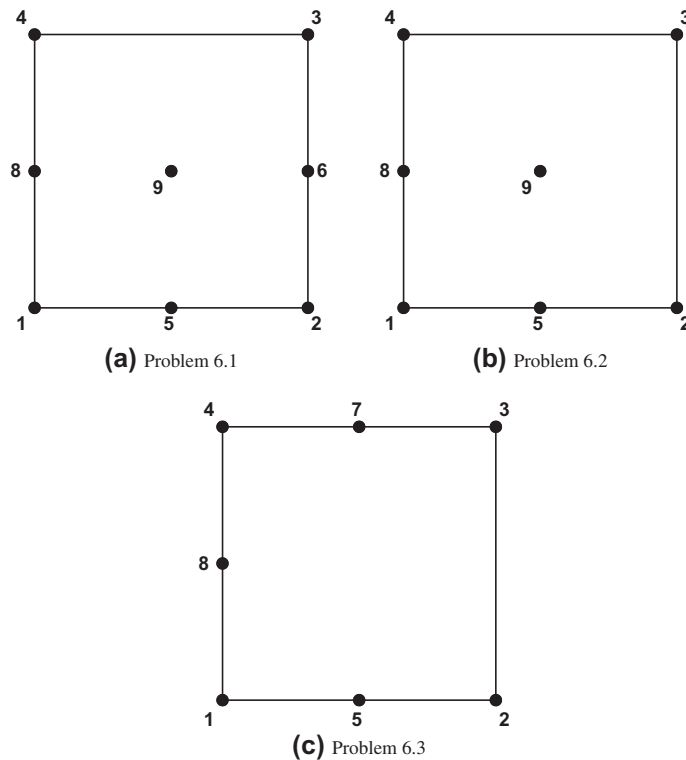
The greatest practical advantage of the use of universal shape function routines is that they can be checked decisively for errors by a simple program with the patch test playing the crucial role (viz. Chapter 8).

The incorporation of simple, exactly integrable, elements in such a system is, incidentally, not penalized as the time of exact and numerical integration in many cases is almost identical.

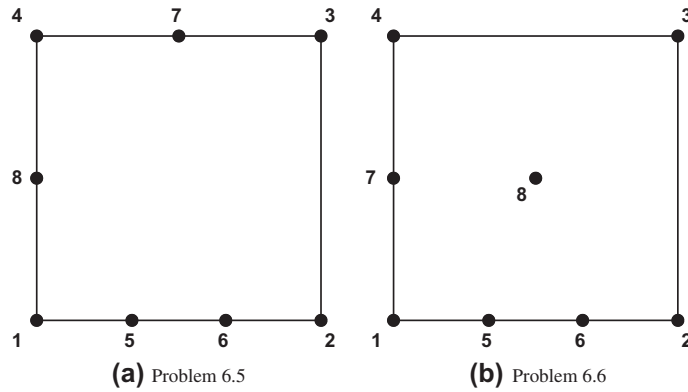
## 6.12 Problems

- 6.1. Develop an explicit form of the standard shape functions at nodes 1, 3, and 6 for the element shown in Fig. 6.32a.  
Using a Pascal triangle in  $\xi$  and  $\eta$  show the polynomials included in the element.
- 6.2. Develop an explicit form of the standard shape functions at nodes 2, 3, and 9 for the element shown in Fig. 6.32b.  
Using a Pascal triangle in  $\xi$  and  $\eta$  show the polynomials included in the element.
- 6.3. Develop an explicit form of the standard shape functions at nodes 1, 2, and 5 for the element shown in Fig. 6.32c.  
Using a Pascal triangle in  $\xi$  and  $\eta$  show the polynomials included in the element.
- 6.4. Compute the parent coordinate first derivatives for the shape functions obtained in Problem 6.3.
- 6.5. Develop an explicit form of the standard shape functions at nodes 1, 2, and 5 for the element shown in Fig. 6.33a.  
Using a Pascal triangle in  $\xi$  and  $\eta$  show the polynomials included in the element.
- 6.6. Develop an explicit form of the standard shape functions at nodes 1, 5, and 7 for the element shown in Fig. 6.33b.  
Using a Pascal triangle in  $\xi$  and  $\eta$  show the polynomials included in the element.

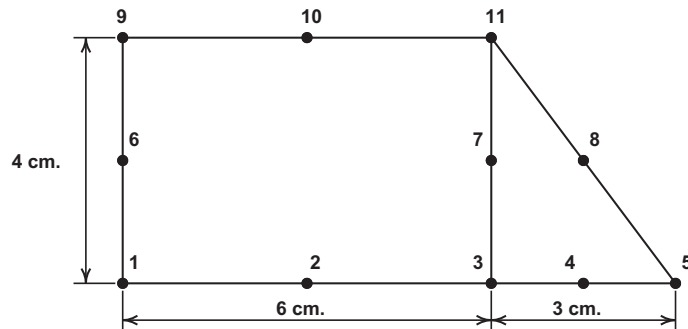
- 6.7** The mesh for a problem contains an eight-node quadratic serendipity rectangle adjacent to a six-node quadratic triangle as shown in Fig. 6.34. Show that the coordinates computed from each element satisfy  $C^0$  continuity along the edge 3-7-11.
- 6.8** Determine an explicit expression for the shape function of node 1 of the linear triangular prism shown in Fig. 6.16a.
- 6.9** Determine an explicit expression for the hierarchical shape function of nodes 1, 7, and 10 of the quadratic triangular prism of Lagrangian family shown in Fig. 6.16b.
- 6.10** Determine an explicit expression for the shape function of nodes 1, 7 and 10 of the quadratic triangular prism of serendipity family shown in Fig. 6.16.
- 6.11** On a sketch show the location of the nodes for the quartic member of the tetrahedron family. Construct an explicit expression for the shape function of the vertex node located at  $(L_1, L_2, L_3, L_4) = (1, 0, 0, 0)$  and the mid-edge node located at  $(0.25, 0.75, 0, 0)$ .

**FIGURE 6.32**

Quadrilateral element for Problems 6.1–6.3.

**FIGURE 6.33**

Quadrilateral element for Problems 6.5 and 6.6.

**FIGURE 6.34**

Quadratic rectangle and triangle for Problem 6.7.

- 6.12** On a sketch show the location of the nodes for the quartic member of the serendipity family. Construct an explicit expression for the shape function of the vertex node located at  $(\xi, \eta, \zeta) = (1, 1, 1)$  and the mid-edge node located at  $(0.75, 1, 1)$ .
- 6.13** On a sketch show the location of the nodes for the cubic member of the triangular prism family shown in Fig. 6.16. Construct an explicit expression for the hierarchical shape function of a vertex node, an edge node of a triangular face, and an edge node of a rectangular face.
- 6.14** On a sketch show the location of the nodes for the quadratic member of the triangular prism family in which Lagrangian interpolation is used on rectangular faces (see Fig. 6.16). Construct an explicit expression for the shape function of a

vertex node, an edge node of a triangular face, and an edge node of a rectangular face.

- 6.15** On a sketch show the location of the nodes for the cubic member of the triangular prism family in which lagrangian interpolation is used on rectangular faces (see Fig. 6.16). Construct an explicit expression for the shape function of a vertex node, an edge node of a triangular face, an edge node of a rectangular face, a mid-face node of a triangular face, a mid-face node of a rectangular face, and for any internal nodes.
- 6.16** A quadratic one-dimensional element is shown in Fig. 6.35 in parent form and in the mapped configuration. Let  $a + b = h$  the total length of the mapped element:
- Determine the shape functions  $N_a(\xi)$  for the three nodes.
  - Plot  $\xi$  vs.  $x$  for values of  $a$  ranging from  $0.2h$  to  $0.8h$  in increments of  $0.1h$ .
  - Plot  $N_a$  vs.  $x$  for the range of  $a$  given in part (b).
  - Plot  $dN_a/dx$  vs.  $x$  for the range of  $a$  given in part (b).
- 6.17** Consider the one-dimensional problem for  $0 \leq x \leq 1$  which is defined by the weak form

$$\int_0^1 \left[ \frac{d\delta u}{dx} \frac{du}{dx} - \delta u q \right] dx - \delta u \sigma \Big|_{x=1} = 0 \quad \text{with } u(0) = 0$$

with  $q = \sigma = 1$ :

- Deduce the Euler differential equation and boundary conditions for the problem.
- Construct an exact solution to the differential equation.
- Solve the weak form using a single quadratic order element with nodes placed at  $x = 0, 5/16$ , and  $1$  and shape functions  $N_a$  defined by:
  - Lagrange interpolation in  $x$  directly
  - Isoparametric interpolation for  $N_a(\xi)$  with  $x = N_a(\xi)\tilde{x}_a$
 Evaluate all integrals using two-point Gaussian quadrature.
- Plot  $u$  and  $du/dx$  for the two solutions. Comment on the differences in quality of the two solutions.

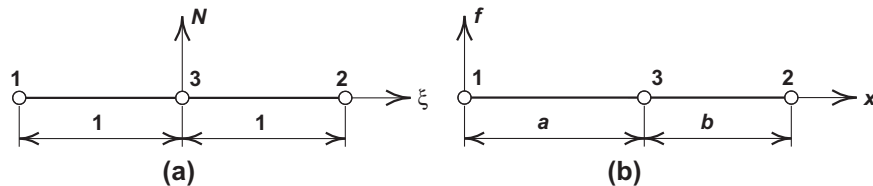


**FIGURE 6.35**

Quadratic element for Problem 6.16: (a) parent element and (b) mapped element.

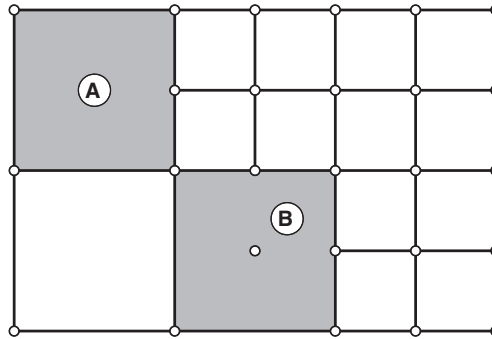
**6.18** It is proposed to create transition elements for use with four-node quadrilateral element meshes as shown in Fig. 6.36:

- (a) Devise the shape functions for the transition element labeled *A*. The shape functions must maintain compatibility along all boundaries. Hint: The element can be a composite form combining more than one four-node element.
- (b) Devise the shape functions for the transition element labeled *B*.
- (c) On a sketch show the location of quadrature points necessary to integrate each element form.
- (d) As an alternative to transition elements, four-node elements may be used for all elements and constraints imposed to maintain compatibility. For the mesh shown in the figure, number all nodes and write the constraint equations necessary to maintain compatibility. The interior node of element *B* is not needed and can be ignored.

**6.19** Determine the hierarchical interpolation functions in  $\xi, \eta$  coordinates for the 16-node cubic order quadrilateral shown in Fig. 6.37a. Express the hierarchic shape functions in a form such that interpolation is given by

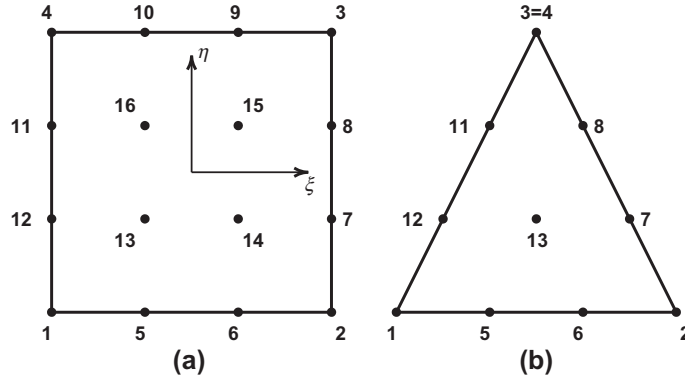
$$f(\xi, \eta) = \sum_{a=1}^4 N_a(\xi, \eta) f_a + \sum_{a=5}^{12} N_a(\xi, \eta) \Delta f_a + \sum_{a=13}^{16} N_a(\xi, \eta) \Delta \Delta f_a$$

**6.20** Determine the hierarchical interpolation functions in  $L_1, L_2, L_3$  area coordinates for the 10-node cubic order triangle shown in Fig. 6.37b. Express your



**FIGURE 6.36**

Transition elements for use with four-node quadrilaterals.

**FIGURE 6.37**

Degeneration of cubic triangle for Problem 6.20: (a) 16-node quadrilateral and (b) 10-node triangle.

hierarchic shape functions in a form such that interpolation is given by

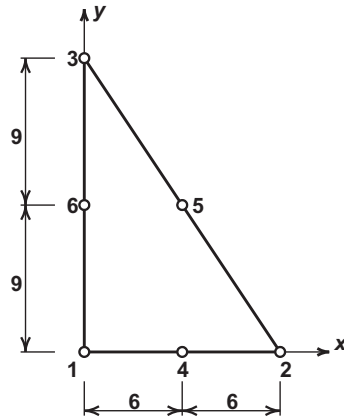
$$f(L_1, L_2, L_3) = \sum_{a=1}^3 N_a(L_1, L_2, L_3) f_a + \sum_{a=5}^8 N_a(L_1, L_2, L_3) \Delta f_a + \sum_{a=11}^{12} N_a(L_1, L_2, L_3) \Delta f_a + N_{13}(L_1, L_2, L_3) \Delta \Delta f_{13}$$

- 6.21** Using the shape functions developed in Problem 6.19, determine the modified shape functions to degenerate the cubic 16-node quadrilateral into the cubic 10-node triangular element using numbering as shown in Fig. 6.37. The final element must be completely consistent with the shape functions developed in Problem 6.20.
- 6.22** Degenerate an eight-node hexahedral element to form a pyramid form with a rectangular base. Write the resulting shape functions for the remaining five nodes.
- 6.23** For the triangular element shown in Fig. 6.38 show that the global coordinates may be expressed in local coordinates as

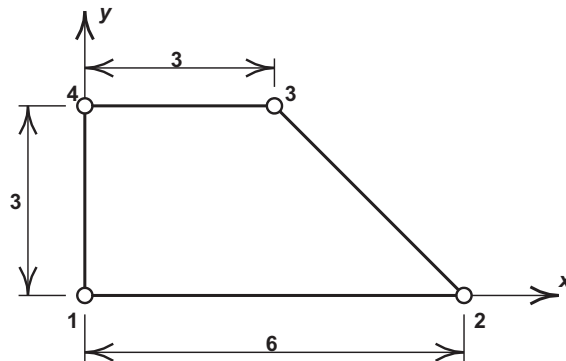
$$\mathbf{x} = \sum_{a=1}^6 N_a(L_b) \tilde{\mathbf{x}}_a = 12 L_2 + 18 L_3$$

- 6.24** For the triangular element shown in Fig. 6.38 compute the integrals  $\int_{\Delta} N_2 N_3 d\Delta$  and  $\int_{\Delta} N_2 N_4 d\Delta$  using:

- (a) Eq. (6.47)  
 (b) An appropriate numerical integration using Table 6.3

**FIGURE 6.38**

Quadratic triangle for Problems 6.23–6.25.

**FIGURE 6.39**

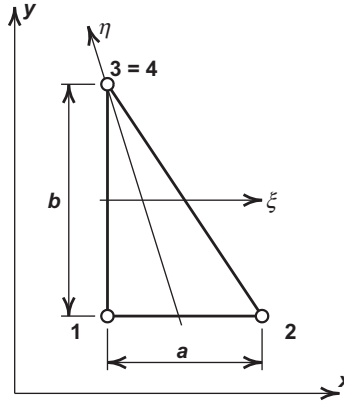
Quadrilateral for Problem 6.26.

**6.25** For the triangular element shown in Fig. 6.38 compute the integrals  $\int_{\Delta} N_a d\Delta$ ;  $a = 1, 2, \dots, 6$  using:

- (a) Eq. (6.47)
- (b) An appropriate numerical integration using Table 6.3

**6.26** The four-node quadrilateral element shown in Fig. 6.39 is used in the solution of a problem in which the dependent variable is a scalar,  $u$ :

- (a) Write the expression for an isoparametric mapping of coordinates in the element.

**FIGURE 6.40**

Degenerate triangle for Problem 6.27.

- (b) Determine the location of the natural coordinates  $\xi$  and  $\eta$  which define the centroid of the element.
- (c) Compute the expression for the Jacobian transformation  $\mathbf{J}$  of the element. Evaluate the Jacobian at the centroid.
- (d) Compute the derivatives of the shape function  $N_3$  at the centroid.

**6.27** A triangular element is formed by degenerating a four-node quadrilateral element as shown in Fig. 6.40. If node 1 is located at  $(x, y) = (10, 8)$  and the sides are  $a = 20$  and  $b = 30$ :

- (a) Write the expressions for  $x$  and  $y$  in terms of  $\xi$  and  $\eta$ .
- (b) Compute the Jacobian  $\mathbf{J}(\xi, \eta)$  for the element.
- (c) Compute the Jacobian determinant  $J(\xi, \eta)$ .
- (d) For a one-point quadrature formula given by

$$I = \int_{-1}^1 \int_{-1}^1 f(\xi, \eta) d\xi d\eta = f(\xi_i, \eta_i) W_i$$

determine the values of  $W_i$ ,  $\xi_i$ , and  $\eta_i$  which exactly integrate the Jacobian  $J$  (and thus also any integral which is a constant times the Jacobian).

- (e) Is this the same point in the element as that using triangular coordinates  $L_a$  and the one-point formula from Table 6.3? If not, why?

**6.28** In some instances it is desirable to perform numerical integration in which quadrature points are located at the end points as well as at interior points. One such formula is Gauss-Lobatto quadrature expressed as

$$\int_{-1}^1 f(\xi) d\xi = [f(-1) + f(1)]W_0 + \sum_{n=1}^N f(\xi_n)W_n$$



Determine the location of the points  $\xi_n$  and the value of the weights  $W_n$  which exactly integrate the highest polynomial of  $f$  possible. Consider:

- (a) The three-point formula ( $n = 1$ )
- (b) The four-point formula ( $n = 2$ )

- 6.29** Write the blending function mapping for a two-dimensional quadrilateral region which has one circular edge and three straight linear edges. Make a clear sketch of the region defined by the function and a  $3 \times 3$  division into four-node quadrilateral elements.
- 6.30** Consider a six-node triangular element with straight edges in which two of the mid-side nodes are placed at the quarter point. Show that the interpolation along the edge produces a derivative which varies as  $1/\sqrt{r}$  where  $r$  is the distance measured from the vertex.
- 6.31** Compute the  $x$  and  $y$  derivatives for the shape function of nodes 1, 7, and 10 of the quadratic triangular prism shown in Fig. 6.16b.
- 6.32** Program development project: Extend the program system started in Problem 5.15 to permit mesh generation using as input a four-node isoparametric block and mapping as described in Section 6.5. The input data should be the coordinates of the block vertices and the number of subdivisions in each direction. Include as an option generation of coordinates in  $r, \theta$  coordinates that are then transformed to  $x, y$  Cartesian form.  
Hint: Once coordinates for all node points are specified, MATLAB can generate a node connection list for three-node triangles using DELAUNAY.<sup>4</sup> A plot of the mesh may be produced using TRIMESH.  
Use your program to generate a mesh for the rectangular beam described in Example 2.3 and the curved beam described in Example 2.4. Note the random orientation of diagonals which is associated with degeneracy in the Delaunay algorithm (viz. Chapter 17).
- 6.33** Program development project: Extend the mesh generation scheme developed in Problem 6.32 to permit specification of the block as a blending function. Only allow two cases: (i) Lagrange interpolation which is linear or quadratic; (ii) circular arcs with specified radius and end points.  
Test your program for the beam problems described in Examples 2.3 and 2.4.

---

## References

- [1] August Möbius, *Der barycentrische, Calcul* (1827), vol. 1, pp. 1–388 (Verlag von S. Hirzel, Leipzig, 1885).
- [2] B.M. Irons, J.G. Ergatoudis, O.C. Zienkiewicz, Comments on ‘complete polynomial displacement fields for finite element method’ (by P.C. Dunne), *Trans. Roy. Aeronaut. Soc.* 72 (1968) 709.

---

<sup>4</sup>In Chapter 17 we discuss mesh generation and some of the difficulties encountered with the Delaunay method.

- [3] J.H. Argyris, I. Fried, D.W. Scharpf, The TET 20 and TEA 8 elements for the matrix displacement method, *Aeronaut. J.* 72 (1968) 618–625.
- [4] R.L. Taylor, On completeness of shape functions for finite element analysis, *Int. J. Numer. Methods Eng.* 4 (1972) 17–22.
- [5] P. Silvester, Higher order polynomial triangular finite elements for potential problems, *Int. J. Eng. Sci.* 7 (1969) 849–861.
- [6] B. Fraeijs de Veubeke, Displacement and equilibrium models in finite element method, in: O.C. Zienkiewicz, G.S. Holister (Eds.), *Stress Analysis*, John Wiley & Sons, Chichester, 1965, pp. 145–197 (Chapter 9).
- [7] J.H. Argyris, Triangular elements with linearly varying strain for the matrix displacement method, *J. Roy. Aeronaut. Soc. Tech. Note* 69 (1965) 711–713.
- [8] J.G. Ergatoudis, B.M. Irons, O.C. Zienkiewicz, Curved, isoparametric, ‘quadrilateral’ elements for finite element analysis, *Int. J. Solids Struct.* 4 (1968) 31–42.
- [9] O.C. Zienkiewicz, B.M. Irons, J.G. Ergatoudis, S. Ahmad, F.C. Scott, Isoparametric and associated elements families for two and three dimensional analysis, in: *Finite Element Methods in Stress Analysis*, Tapir Press, Trondheim, 1969 (Chapter 13).
- [10] J.H. Argyris, K.E. Buck, H.M. Hilber, G. Mareczek, D.W. Scharpf, Some new elements for matrix displacement methods, in: *Proceedings of the Second Conference on Matrix Methods in Structural Mechanics*, vol. AFFDL-TR-68-150, Wright Patterson Air Force Base, Ohio, October 1968.
- [11] O.C. Zienkiewicz, B.M. Irons, J. Campbell, F.C. Scott, Three dimensional stress analysis, in: *IUTAM Symposium on High Speed Computing in Elasticity*, Liège, 1970.
- [12] F.C. Scott, A quartic, two-dimensional isoparametric element, Undergraduate Project, University of Wales, 1968.
- [13] J.G. Ergatoudis, B.M. Irons, O.C. Zienkiewicz, Three dimensional analysis of arch dams and their foundations, in: *Proceedings of the Symposium on Arch Dams*, Institution of Civil Engineers, London, 1968.
- [14] I.C. Taig, Structural analysis by the matrix displacement method, Technical Report, Report No. S.0.17, English Electric Aviation Ltd., April 1962. Based on work performed 1957–1958.
- [15] E.L. Wachspress, High order curved finite elements, *Int. J. Numer. Methods Eng.* 17 (1981) 735–745.
- [16] M. Crochet, Personal communication, 1988.
- [17] Nam-Sua Lee, K.-J. Bathe, Effects of element distortion on the performance of isoparametric elements, *Int. J. Numer. Methods Eng.* 36 (1993) 3553–3576.
- [18] R. Radau, Études sur les formules d’approximation qui servent à calculer la valeur d’une intégrale définie, *J. Math. Pures Appl.* 6 (1880) 283–336.
- [19] R.G. Anderson, B.M. Irons, O.C. Zienkiewicz, Vibration and stability of plates using finite elements, *Int. J. Solids Struct.* 4 (1968) 1033–1055.
- [20] P.C. Hammer, O.P. Marlowe, A.H. Stroud, Numerical integration over symplexes and cones, *Math. Tables Aids Comput.* 10 (1956) 130–137.
- [21] C.A. Felippa, Refined finite element analysis of linear and non-linear two-dimensional structures, Ph.D. dissertation, Department of Civil Engineering,

- SEMM, University of California, Berkeley, 1966. Also SEL Report 66-22, Structures Materials Research Laboratory.
- [22] M. Abramowitz, I.A. Stegun (Eds.), *Handbook of Mathematical Functions*, Dover Publications, New York, 1965.
- [23] G.R. Cowper, Gaussian quadrature formulas for triangles, *Int. J. Numer. Methods Eng.* 7 (1973) 405–408.
- [24] J.N. Lyness, D. Jespersen, Moderate degree symmetric quadrature rules for the triangle, *J. Inst. Math. Appl.* 15 (1975) 19–32.
- [25] B.M. Irons, Engineering applications of numerical integration in stiffness methods, *J. AIAA* 4 (1966) 2035–2037.
- [26] G. Strang, G.J. Fix, *An Analysis of the Finite Element Method*, Prentice-Hall, Englewood Cliffs, NJ, 1973.
- [27] I. Fried, Accuracy and condition of curved (isoparametric) finite elements, *J. Sound Vibr.* 31 (1973) 345–355.
- [28] I. Fried, Numerical integration in the finite element method, *Comput. Struct.* 4 (1974) 921–932.
- [29] M. Zlamal, Curved elements in the finite element method, *SIAM J. Numer. Anal.* 11 (1974) 347–362.
- [30] D. Kosloff, G.A. Frasier, Treatment of hour glass patterns in low order finite element codes, *Int. J. Numer. Anal. Methods Geomech.* 2 (1978) 57–72.
- [31] T. Belytschko, W.E. Bachrach, The efficient implementation of quadrilaterals with high coarse mesh accuracy, *Comput. Methods Appl. Mech. Eng.* 54 (1986) 276–301.
- [32] R.E. Newton, Degeneration of brick-type isoparametric elements, *Int. J. Numer. Methods Eng.* 7 (1974) 579–581.
- [33] B.M. Irons, A technique for degenerating brick type isoparametric elements using hierarchical midside nodes, *Int. J. Numer. Methods Eng.* 8 (1974) 209–211.
- [34] O.C. Zienkiewicz, D.V. Phillips, An automatic mesh generation scheme for plane and curved surfaces by isoparametric coordinates, *Int. J. Numer. Methods Eng.* 3 (1971) 519–528.
- [35] W.J. Gordon, C.A. Hall, Construction of curvilinear co-ordinate systems and application to mesh generation, *Int. J. Numer. Methods Eng.* 3 (1973) 461–477.
- [36] W.J. Gordon, C.A. Hall, Transfinite element methods – blending-function interpolation over arbitrary curved element domains, *Numer. Math.* 21 (1973) 109–129.
- [37] L. Piegl, W. Tiller, *The NURBS Book (Monographs in Visual Communication)*, second ed., Springer-Verlag, New York, 1997.
- [38] G. Farin, *Curves and Surfaces for CAGD: A Practical Guide*, fifth ed., Morgan Kaufmann Publishers, San Francisco, CA, 2002.
- [39] D.F. Rogers, *An Introduction to NURBS: With Historical Perspective*, Academic Press, San Diego, 2000.
- [40] B.M. Irons, Economical computer techniques for numerically integrated finite elements, *Int. J. Numer. Methods Eng.* 1 (1969) 201–203.